JOURNAL OF GEOPHYSICAL RESEARCH, VOL. 100, NO. D5, PAGES 9041-9071, MAY 20, 1995

A three-dimensional general circulation model with coupled chemistry for the middle atmosphere

P.J. Rasch, B.A. Boville, and G.P. Brasseur

National Center for Atmospheric Research, Boulder, Colorado

Abstract. We document a new middle atmosphere general circulation model that includes ozone photochemistry. The dynamical model component is based on the NCAR middle atmosphere version of the Community Climate Model. The chemistry model component simulates the evolution of 24 chemically reactive gases. The horizontal resolution is approximately 3° in latitude and 6° in longitude. It includes 44 levels, with a maximum vertical grid spacing of about 2.5 km and a top level at around 75 km. The chemical model distinguishes between species where we judge transport to be critical and those for which it may be neglected. Nine longer-lived species (N_2O, CH_4, H_2O, HNO_3, N_2O_5, CO, $ClONO_2$, HCl, and HOCl) and four chemical families (NO_y, NO_x, O_x and Cl_x) are advected. Concentrations of 15 species which are typically shorter-lived or are members of the chemical families are diagnosed using quasi-equilibrium assumptions ($O(^1D)$, OH, Cl, $O(^3P)$, O_3, HO_2, NO_2, ClO, NO, HNO_4, NO_3, N, OClO, Cl_2O_2, H_2O_2). Distributions for a number of other species are prescribed. Results are presented from a 2-year simulation, which include only gas phase photochemical reactions and in which the ozone distribution forecast from the chemistry module does not affect the radiative forcing of the dynamical fields. The calculated distributions of trace species and their seasonal evolution are often quite realistic, particularly in the northern hemisphere extratropics. Distributions of long-lived species such as N_2O and CH_4 correspond well to satellite observations. Some features, such as the double peak structure occurring during equinoxes, are not reproduced. The latitudinal variation and seasonal evolution of the ozone column abundance is quite realistic. The calculated vertical distribution of the ozone mixing ratio exhibits significant differences from measured values. The model underestimates significantly the ozone in the upper stratosphere (40 km) and in the extratropics, where the maximum values occur at too low an altitude. The model reproduces the key features expected in the distribution of fast reacting nitrogen and chlorine compounds. Problems in the southern polar simulation (which we attribute to the lack of a comprehensive parameterization of gravity waves) are discussed. The model currently parameterizes only stationary gravity waves generated by flow over orography. Other sources of gravity waves may be required to improve the model simulation.

1. Introduction

In this paper we present initial results from multiyear integrations of a model containing a relatively comprehensive representation of the dynamics and thermodynamics of the atmosphere from the surface through the middle atmosphere and much of the chemistry relevant to the middle atmosphere. We believe the time has come to attempt to couple comprehensive General Circulation Models (GCMs) with equally comprehensive chemistry models, and our initial attempt at this coupling takes place in the context of a study of the middle atmosphere, where both the dynamics and the chemistry are less strongly influenced by the very complicated physical processes connected with phase changes of water and with the interaction between the atmosphere and those components of the Earths' system near the surface (oceans, biosphere, lithosphere).

The effects of coupling the chemistry and dynamics of the stratosphere can be important throughout the climate system. The middle atmosphere is the place where the largest changes of anthropogenic origin in the Earth's climate are occurring. A gradual cooling has been seen in the temperature of the middle atmosphere, thought to be due to increasing greenhouse gases [*Chanin*, 1993], or the recent changes in ozone amounts. In addition to the direct effect of additional

Paper number 95JD00019.
0148-0227/95/95JD-00019$05.00

greenhouse gases, perturbations of ozone photochemistry due to the release of Chlorofluorocarbons (CFCs) and the anthropogenic production of ozone in the troposphere have introduced a significant change in both the latitudinal and the vertical distribution of ozone [*World Meteorological Organization (WMO)*, 1985; *Ramaswamy et al.*, 1992; *Wang et al.*, 1993]. The resulting changes in the vertical and latitudinal distribution of thermal forcing influence the general circulation and have an attendant effect on the transport of heat, momentum, and trace species. For example, latitudinal changes in the ozone distribution (i.e., the ozone hole) can lead to substantial changes in the persistence and strength of the polar vortex and thus enhance the effect of the CFCs in ozone reduction in polar regions [*Kiehl et al.*, 1988]. *Rind et al.* [1990] have shown that the middle atmosphere response to CO_2 doubling is quite subtle. Although the general trend of a warmer troposphere/cooler stratosphere was found, a warming was found in the northern hemisphere polar stratosphere during winter. This is clearly not in agreement with the first-order radiative response and may have important implications for ozone depletion in the northern hemisphere winter by heterogeneous chemistry in the presence of polar stratospheric clouds (PSCs). The warming was a result of the changed dynamical heating associated with the change in the residual circulation. The result was sensitive to the latitudinal distribution of the sea surface temperature perturbation associated with the CO_2 doubling.

In addition to changes in the middle atmosphere circulation, theoretical results [e.g., *Geller and Alpert, 1980*] and modeling studies [e.g., *Hansen et al.*, 1983; *Boville*, 1984] demonstrate a tropospheric response to perturbations in the stratospheric dynamics. Both the stationary and the transient components of tropospheric wave structures can be modulated by the stratospheric circulation. *Kodera et al.* [1991] and *Kodera* [1993] demonstrated that anomalies initially created in the stratosphere can propagate into the troposphere through wave-mean flow interactions. Because the troposphere is the fundamental source of wave energy for the middle atmosphere, these studies suggest that it is important to begin to study the complex feedbacks taking place between the stratosphere and the troposphere through temperature, ozone, and wave effects.

In attempts to understand a complex process, it is generally advantageous to isolate one component of the system and simplify those other components that are peripheral to the area of focus. This has historically been the approach taken in studies of the Earth's climate. For example, in most "comprehensive" general circulation models the distribution of radiatively active trace gases is prescribed, rather than calculated within the model (with the exception of the H_2O distribution). Traditionally, ocean temperatures, the influence of biota on albedo, and soil respiration are also prescribed. In virtually all models focusing on the middle atmosphere, the formulation of physical and chemical processes occurring in the troposphere is greatly simplified; often when the chemistry is treated in great detail, the dynamical and physical representations are crudely represented. These simplifications have the benefit of leading to faster programs. The simple parameterizations of important processes always lead to the introduction of free parameters, which must be adjusted to tune the models behavior. They often cut out feedback loops of potential importance by fixing features (either deemed too complex or not of current interest) to climatologically representative values, hence reducing the variability of the resulting system.

With more comprehensive models, physical processes are treated more realistically, and a larger set of feedback loops are taken into account, allowing the possibility of new behavior not seen in the simpler models. Initial attempts at coupling sophisticated ocean and atmospheric models began in the early 1960s [*Manabe and Bryan*, 1969]. Somewhat later, sophisticated surface models were coupled to GCMs [*Sellers et al.*, 1986; *Dickinson et al.*, 1987]. Allowing new processes and new feedbacks in a model can sometimes produce unexpected responses, highlighting areas requiring more attention. These areas sometimes point to a lack of understanding about the processes through which the interactions take place and sometimes to internal inadequacies of the component models. Nevertheless, substantial progress takes place, with a corresponding increase in knowledge about the component processes and their interactions.

We are certainly not the first to attempt to model the interaction between the chemistry and the dynamics of the middle atmosphere. The field has a large and well-developed history, but like the other segments of climate modeling, the field has often treated one set of processes in great detail, to the neglect of others.

Two-dimensional (latitude/height) chemical transport models, with highly parameterized dynamics, lie at one end of the spectrum of these efforts. Transport is typically represented by a combination of a residual mean circulation to account for large-scale processes and an eddy diffusivity to account for transient and unresolved mixing processes. Examples of these type of models include *Harwood and Pyle* [1975], *Nicoli and Visconti* [1982], *Garcia and Solomon* [1983], *Garcia et al.* [1992], *Stordal et al.* [1985], *Brasseur et al.* [1990], *Ko et al.* [1984], *Jackman et al.* [1991], and *Yang et al.* [1991]. Because of their computational efficiency these models are commonly used for assessment studies of potential ozone changes in the stratosphere.

At the other end of the spectrum lie models with more detailed dynamical and radiative formulations and simpler chemistry. The role of dynamics in controlling the distribution of idealized trace species with extremely simple chemical representations has been investigated in the context of General Circulation Models (GCMs) and in transport models, which use prescribed meteorological data to drive a chemical transport calculation. Examples can be found in the works of *Mahlman and Moxim* [1978], *Mahlman and Umscheid* [1984], *Sassi et al.* [1993], *Rasch et al.* [1993]. Coupling of relatively

comprehensive photochemistry in a three-dimensional transport model using GCM data was performed by *Grose et al.* [1987]. Recently, *Lefèvre et al.* [1994] have included a more comprehensive photochemistry model for short integrations in a three-dimensional chemical transport model, using data taken from atmospheric analyses. Mechanistic models, using a simplified representation of the troposphere with a relatively comprehensive chemistry calculation, have been made by *Rose and Brasseur* [1989]. *Cariolle and Déqué* [1986] and *Cariolle et al.* [1990] have included a linearized photochemical formulation relevant for the middle atmosphere. *Pitari et al.* [1992] have included a comprehensive chemical representation in a very simple 3-D model with a relatively crude radiative and dynamical representation. A similar study has been made by *Austin et al.* [1992] that included ozone radiative feedbacks and a more realistic temperature distribution, but their integrations were performed only over relatively short time periods.

In this paper we document a new model comprised of two components: a middle atmosphere general circulation model (the National Center for Atmospheric Research (NCAR) middle atmosphere version of the Community Climate Model (CCM), version 2) and an ozone chemistry model. This model simulates the evolution of 24 chemically reactive gases, including ozone. Although there are many fewer gross assumptions about the free atmosphere in GCMs than in the simpler middle atmosphere models, the most obvious remaining inadequacies are associated with the treatment of clouds (the parameterization of moist processes, trace species transport, and the radiative properties of clouds) and in the treatment of the subgrid scale dynamical processes which exert a strong control on the resolved scale motions (i.e., the momentum transport and deposition associated with gravity wave processes whose source arises from flow over orography, convection, shear instabilities, and the propagation of fronts).

Our chemical model distinguishes between species where we judge transport to be critical (we call them longer-lived species) and those for which it may be neglected (hereafter shorter-lived species). Nine long-lived species and four chemical families are advected. Concentrations of 15 species which are typically shorter-lived or are members of the chemical families are diagnosed using quasi-equilibrium assumptions. (The distinction between long- and short-lived species is necessarily somewhat arbitrary). Distributions for a few other species are prescribed (e.g., N_2, O_2). So far, we have restricted our attention only to gas phase reactions. It is clear that the chemistry taking place on the surface of particles must also be included in order to simulate the lower stratosphere realistically.

Despite remaining inadequacies in all components of the system, we believe that the model represents a substantial step toward a comprehensive coupled climate/chemistry system. The GCM component is substantially more complex and realistic than the 2-D models mentioned above. Because the winds and temperature fields can respond to the distributions of the radiatively active trace gases, there is the possibility of climate feedbacks which are absent in the chemistry transport models using prescribed winds and temperatures (although in this paper we will not discuss the results in which the photochemistry feeds back on the model dynamics). The model is efficient enough so that multiyear integrations are possible, and climate/chemistry interactions may be studied. It is our intent here to provide a description of the behavior of some aspects of this very complex model. The simulations serve to highlight what we are capable of modeling, and where more work is required. Many aspects of the simulation look quite promising. Some problems point to a lack of understanding about the processes through which the interactions take place and some to internal inadequacies of the component models. The paper is organized as follows: in section 2 we describe the component models in some detail; section 3 describes the mode in which the model is integrated; section 4 displays results from the integration; section 5 summarizes highlights from the study.

2. Model Description

2.1. Atmospheric Component: NCAR Middle Atmosphere Community Climate Model Version 2 (MACCM2)

The NCAR Community Climate Model, version 2 (hereinafter referred to as CCM2), is a descendant of the various earlier versions of the NCAR CCM [*Williamson et al.*, 1987; *Boville and Randel*, 1992]. The CCM2 was originally developed and tuned as a tropospheric model, but one of the design requirements was that minimal changes to the model would be necessary to use it in either tropospheric or middle atmospheric form. The standard tropospheric version of CCM2 is described by *Hack et al.* [1993]. The extension to the middle atmospheric version is achieved through minor modifications to the model. The vertical domain is extended (to 75 km), and resolution is changed (to a maximum of 2.5 km vertical spacing), as is the horizontal resolution (5.6° in the east/west direction and 2.8° in the north/south direction) and the frequency at which the absorptivities and emissivities are calculated. There are also a few other changes made to the model parameters to ease the computational expense. We will briefly document the basic characteristics of the model in this section, and highlight the few places where CCM2 and the NCAR Middle Atmosphere Community Climate Model Version 2 (MACCM2) differ in formulation, or model climatology. The model climatology is described much more thoroughly in a companion paper [*Boville*, this issue]. Additional comments regarding the simulation can be found in the work of *Rasch et al.* [1993].

The evolution equations for heat and momentum use a spectral representation for the horizontal treatment and first-order vertical finite differences for vertical gradients. A hybrid vertical coordinate is used that is ter-

rain following in the lower troposphere and gradually makes a transition to a pressure following coordinate in the lower stratosphere. The time integration scheme used for the dynamical and thermodynamic equation is a semi-implicit, leapfrog time integration scheme.

The transport of moisture and tracer species is done using a three-dimensional "shape-preserving" semi-Lagrangian transport formalism. The transport scheme was originally developed for the transport of water vapor in the troposphere [*Rasch and Williamson*, 1990, 1991]. More recently it has been used for the simulation of stratospheric aerosol transport [*Boville et al.*, 1991], the transport of radioactive isotopes [*Rasch et al.*, 1993], and the transport of CFCs in the troposphere [*Hartley et al.*, 1994]. Because the shape-preserving transport algorithm can maintain very sharp gradients without introducing overshoots or undershoots and diffuses only at the smallest scales of the model, no additional horizontal diffusion is needed on the model tracers. The semi-Lagrangian transport is not inherently conservative, and a mass correction, which we term a "mass fixer", must be applied to the solution at the end of each time step to strictly enforce this conservation. Because the original semi-Lagrangian transport algorithms were developed for water vapor, we have encountered a number of minor problems in its use in transporting species in the middle atmosphere. Minor modifications have been made to the algorithms to make them more appropriate for the transport of trace species. These modifications are detailed in the appendix. Briefly, we have modified the transport algorithm to move trace species mixing ratios normalized by "dry air" mass, rather than original formulations use of mixing ratios normalized by "moist air" mass, and we have modified the original fixer to reduce its impact on tracers in which most of the mass is concentrated in the middle atmosphere, unlike water vapor.

The planetary boundary layer (PBL) parameterization [*Holtslag and Boville*, 1993] is a nonlocal scheme, in which the boundary layer depth is calculated explicitly, and the profile of diffusion coefficients is prescribed below that depth. The parameterization includes the typical down gradient diffusion throughout the depth of the atmosphere as well as a less typical nonlocal transport term within the convective boundary layer (sometimes called a countergradient transport term). Above the boundary layer a local vertical diffusion scheme is used, with a local Richardson-number-dependent diffusion coefficient. A parameterization of momentum flux divergence (produced by stationary gravity waves arising from flow over orography) is included. In addition, the breaking of gravity waves in the mesosphere is treated through a Rayleigh friction term that becomes important above 60 km.

A mass flux scheme [*Hack*, 1994] is used to represent all types of moist convection. The convective scheme moves heat, moisture, and trace species in a self-consistent way. The cloud fraction and cloud albedo parameterizations depend on relative humidity, vertical motion, static stability, and precipitation rate. Clouds are permitted at all tropospheric levels above the surface layer. The cloud emissivities are determined from a prescribed liquid water path, which is a function of latitude.

The solar radiative heating is computed using a Δ-Eddington parameterization with 18 spectral bands [*Briegleb*, 1992]. The longwave calculation includes a Voigt line shape correction (incorporated to increase cooling rates in the upper stratosphere and mesosphere). Radiative heating rates are calculated at 6-hour intervals and held constant between calculations. Absorptivities and emissivities are calculated every 12 hours. Radiatively active gases accounted for in the model include O_3, CO_2, and H_2O. The model assumes a fixed value of $CO_2 = 330$ ppmv. O_3 values used in the radiative calculation are prescribed based on a linear interpolation of monthly mean, zonally averaged values from a combination of data from the Limb Infrared Monitor of the Stratosphere (LIMS) [*Gille and Lyjak*, 1986] merged with Solar Mesosphere Explorer (SME) data above 0.1 mbar. H_2O values vary at each time step in the model and influence the absorptivity and emissivity calculations. The land temperature is calculated by a four-layer diffusion model with soil heat capacities specified for each layer to capture the major observed climatological cycles. The land has specified soil hydrologic properties. Sea surface temperatures are specified by linear interpolation between the climatological monthly mean values. Surface fluxes are calculated with stability-dependent transfer coefficients between the surface and the first model level.

The MACCM2 simulation is quite reasonable but suffers from some of the same problems seen in other stratospheric GCMs and in earlier versions of the stratospheric CCM [e.g., *Boville and Randel*, 1986, 1992]. The general characteristics of the simulation are treated in much more detail by *Boville* [this issue]. We outline some of the important characteristics here; others will be described in later sections.

The zonal mean climatology for the northern hemisphere is reasonably realistic for all seasons, although the northern hemisphere polar night jet is somewhat too far poleward and too strong. The southern hemisphere polar temperatures are too cold by 30° to 40° in the middle and upper stratosphere, with a concomitant polar night jet which is at least 50 m s^{-1} too strong. These errors are thought to be due to the lack of an appropriate source of momentum transport associated with gravity waves which are probably generated by shear and convective instabilities and the propagation of fronts [*Garcia and Boville*, 1994]. The interannual variability of the zonal mean temperatures and winds in northern high latitudes is realistic. The simulation in the tropics is less satisfactory. The model is capable of simulating some aspects of the semiannual oscillation (SAO) seen in the upper stratosphere and mesosphere zonal winds. The easterly phase of the SAO is well represented. The westerly phase is too weak [*Sassi et al.*, 1993]. The model does not simulate the quasi-biennial oscillation (QBO), which is thought to arise through

the driving by very short vertical scale equatorial waves. The model is generally in a mode similar to the easterly phase of the QBO seen in the atmosphere.

2.2. Chemistry Component: Middle Atmosphere Chemistry Model

The chemical scheme used in the model includes 24 species and 85 chemical/photochemical reactions. To avoid the numerical problems associated with "stiff" mathematical systems, several fast-reacting compounds have been grouped into overlapping chemical families, i.e., $NO_x = NO + NO_2$; $NO_y = ClONO_2 + NO_x + HNO_3 + 2N_2O_5 + HNO_4 + NO_3 + N$; $O_x = O_3 + O(^3P) + O(^1D)$ and $Cl_x = Cl + ClO + OClO + 2Cl_2O_2 + HCl + ClONO_2 + HOCl$. These families are advected together with longer-lived species, i.e., N_2O, CH_4, H_2O, HNO_3, N_2O_5, HCl, $ClONO_2$, HOCl, and *CO*. The concentrations of the individual members of chemical families as well as of other shorter-lived species (i.e., OH, HO_2, NO_2, HNO_4, H_2O_2) are diagnosed using equilibrium assumptions.

The concentrations of the principal atmospheric constituents are prescribed (N_2 = 78% and O_2 = 20%), while for H_2, a relatively inert species in the troposphere and stratosphere, a constant mixing ratio of 500 ppbv is adopted. A specified concentration of 10 pptv is adopted for BrO during daytime. It is reduced to 1 pptv during nighttime. To reduce the complexity of the chemical scheme, while retaining the ability to consider different levels of perturbations by several anthropogenic halocarbons, we have prescribed the source of inorganic chlorine in the stratosphere by constraining the total amount of Cl_x in the upper stratosphere. In this particular run, the Cl_x mixing ratio has been capped at 4 ppbv. To reproduce the vertical and latitudinal distribution of the Cl_x source, we have used the 2-D distributions of the three dominant gases ($CFCl_3$, CF_2Cl_2, and CH_3Cl) predicted by the 2-D model of *Brasseur et al.* [1990] and have scaled them by a factor of 1.8, 1.4, and 1.0, respectively, to account for other halocarbons. This value of available chlorine is higher than seen at the present time and might be more appropriate to the next decade. In future runs we will transport these species to provide more consistent and realistic Cl_x distributions.

The photolysis coefficients are taken from a precalculated lookup table as functions of the pressure level (and hence O_2 column abundance), the ozone column, the solar zenith angle, and the albedo. The treatment of the Schumann-Runge bands is based on the formulation of *Kockarts* [1976]. The photolysis of NO in the delta bands uses the formulation of *Nicolet* [1979]. In this first version of the model, heterogeneous reactions on the surface of particles in polar stratospheric clouds and of sulfate aerosols are ignored. Removal of NO_y and Cl_x by washout processes in the troposphere is crudely parameterized by including an additional destruction rate, based on the results provided by the 2-D model of *Brasseur et al.* [1990] below 12 km in altitude. The corresponding washout frequency for NO_y is chosen to be equal to 2×10^{-8} s^{-1} near the surface and to decrease as a function of height with a scale height of 14 km. In the case of Cl_x the surface value is 6×10^{-9} s^{-1}, and the scale height is 5 km. The lower boundary conditions (applied at the surface) for the transported species are specified as prescribed mixing ratios taken from the 2-D model of *Brasseur et al.* [1990]. At the top of the model near 75 km, NO_x (and hence NO_y) is set to 5 ppbv and CO to 0.5 ppmv. Mixing ratios for other species are unchanged during inflow from above and are updated to the departure point value otherwise.

The chemical reactions included in the model are given in Tables 1a and 1b. Rate constants are determined following *DeMore et al.* [1990] with a few modifications. The reactions for species undergoing photolysis are listed in Table 2.

The evolution equations for trace species are solved by the method of operator splitting. First, the semi-Lagrangian transport method is used to account for the advection process (with the mass conservation constraint enforced). Chemical tendencies are then calculated and used to modify the distributions. Following the update by chemistry, diffusion by vertical subgrid-scale processes, then redistribution by convection is applied. This completes a time step, and the process is then repeated until the integration is complete.

To illustrate the numerical method used to calculate the tendencies from chemical processes, consider the continuity equation

$$\frac{\partial q}{\partial t} = P - Lq$$

where q is a number density (cm^{-3}) for a species; P is the production term (cm^{-3} s^{-1}); and L is a loss rate (s^{-1}). The computer codes have been designed to be able to use any of a variety of numerical methods to solve this equation. The solutions appearing in this paper use a simple implicit (Euler backward) formulation for the advected species:

$$q^{new} = \frac{q^{old} + P^{old}\Delta t}{1 + L^{old}\Delta t}. \quad (1)$$

We use the semianalytic method proposed by *Hesstvedt et al.* [1978] for the nonadvected species,

$$q^{new} = \begin{cases} (q^{old} - P^{old}/L^{old})e^{-L^{old}\Delta t} + P^{old}/L^{old} & L > 0 \\ q^{old} + P^{old}\Delta t & L = 0 \end{cases},$$

which is somewhat more accurate than (1) for species with very large loss rates.

3. Description of Model Run

The primary mode of coupling between the chemical and the dynamical model components is through the water vapor and ozone distributions. In the original MACCM2, these species were controlled both by

the dynamics and by the physical processes present (for H_2O) or were prescribed as mentioned above (for CO_2 and O_3). The chemical source from methane oxidation for H_2O can be explicitly included in our new model, and O_3 can be controlled by both transport and chemistry through the reactions described above. The chemical source/sink terms can feed back on the dynamics through their effect on the radiative forcing, which drives the temperature distribution. In addition to the transport feedback, there is also a feedback through the temperature dependence of the rate constants.

Our new model can be run with various degrees of

Table 1a. Chemical Reactions Included in the Model

Rate Coefficient, $cm^3\ s^{-1}$	Reaction
$a_1 = 5.7 \times 10^{-32}[M](300/T)^{1.6}$	$H + O_2 + M \rightarrow HO_2 + M$
$a_{1et} = 2.2 \times 10^{-10}$	$O(^1D) + H_2O \rightarrow OH + OH$
$a_2 = 1.4 \times 10^{-10}\ \exp(-470/T)$	$H + O_3 \rightarrow O_2 + OH$
$a_{3et} = 1.0 \times 10^{-10}$	$O(^1D) + H_2 \rightarrow OH + H$
$a_5 = 2.2 \times 10^{-11} \exp(120/T)$	$OH + O(^3P) \rightarrow O_2 + H$
$a_6 = 1.6 \times 10^{-12} \exp(-940/T)$	$OH + O_3 \rightarrow HO_2 + O_2$
$a_{6b} = 1.1 \times 10^{-14} \exp(-500/T)$	$HO_2 + O_3 \rightarrow OH + 2O_2$
$a_7 = 3.0 \times 10^{-11} \exp(200/T)$	$HO_2 + O(^3P) \rightarrow OH + O_2$
$a_{17} = 4.8 \times 10^{-11} \exp(250/T)$	$HO_2 + OH \rightarrow H_2O + O_2$
$a_{19} = 5.5 \times 10^{-12} \exp(-2000/T)$	$OH + H_2 \rightarrow H_2O + H$
$a_{23a} = 7.3 \times 10^{-11}$	$H + HO_2 \rightarrow 2OH$
$a_{23b} = 6.5 \times 10^{-12}$	$H + HO_2 \rightarrow H_2 + O_2$
$a_{23c} = 1.6 \times 10^{-12}$	$H + HO_2 \rightarrow H_2O + O(^3P)$
$a_{26} = 3.7 \times 10^{-12} \exp(240/T)$	$NO + HO_2 \rightarrow OH + NO_2$
$a_{27} = 2.3 \times 10^{-13} \exp(600/T)$	$HO_2 + HO_2 \rightarrow O_2 + H_2O_2$
$a_{30} = 2.9 \times 10^{-12} \exp(-160/T)$	$H_2O_2 + OH \rightarrow H_2O + HO_2$
$a_{36} = 1.5 \times 10^{-13}(1 + 0.6P(mb)/1013)$	$OH + CO \rightarrow CO_2 + H$
$b_3 = 6.5 \times 10^{-12} \exp(120/T)$	$O(^3P) + NO_2 \rightarrow NO + O_2$
$b_4 = 2.0 \times 10^{-12} \exp(-1400/T)$	$O_3 + NO \rightarrow NO_2 + O_2$
$b_6 = 3.4 \times 10^{-11}$	$N + NO \rightarrow N_2 + O$
$b_7 = 1.5 \times 10^{-11} \exp(-3600/T)$	$N + O_2 \rightarrow NO + O(^3P)$
$b_9 = 1.2 \times 10^{-13} \exp(-2450/T)$	$O_3 + NO_2 \rightarrow NO_3 + O_2$
$b_{24} = b_{23}/2.1 \times 10^{-27}[M](10900/T)+$	$HO_2NO_2 + M \rightarrow HO_2 + NO_2 + M$
$b_{27} = 7.2 \times 10^{-15} \exp(785/T)$ $+\frac{1.9\times10^{-33}\exp(725./T)[M]}{1.+1.9\times10^{-33}\exp(725./T)[M]/(4.1\times10^{-16}\exp(1440./T)}$	$HNO_3 + OH \rightarrow H_2O + NO_3$
$b_{28} = 1.3 \times 10^{-12} \exp(380/T)$	$HO_2NO_2 + OH \rightarrow H_2O + NO_2 + O_2$
$b_{32} = b_{12}/4 \times 10^{-27}[M] \exp(-10930/T)$	$N_2O_5 + M \rightarrow NO_3 + NO_2 + M$
$b_{38} = 4.9 \times 10^{-11}$	$N_2O + O(^1D) \rightarrow N_2 + O_2$
$b_{39} = 6.7 \times 10^{-11}$	$N_2O + O(^1D) \rightarrow 2NO$
$c_1 = 1.4 \times 10^{-10}$	$O(^1D) + CH_4 \rightarrow ... \rightarrow CO + 2H_2O$
$c_2 = 3.9 \times 10^{-12} \exp(-1885/T)$	$CH_4 + OH \rightarrow ... \rightarrow CO + 2H_2O + HO_2$
$d_0 = 2.1 \times 10^{-12} \exp(-1150/T)$	$CH_3Cl + OH \rightarrow Cl +$ products
$d_2 = 2.9 \times 10^{-11} \exp(-260/T)$	$O_3 + Cl \rightarrow ClO + O_2$
$d_3 = 3.0 \times 10^{-11} \exp(70/T)$	$O(^3P) + ClO \rightarrow Cl + O_2$
$d_4 = 6.4 \times 10^{-12} \exp(290/T)$	$NO + ClO \rightarrow Cl + NO_2$
$d_5 = 1.1 \times 10^{-11} \exp(-1400/T)$	$Cl + CH_4 \rightarrow CH_3 + HCl$
$d_6 = 3.7 \times 10^{-11} \exp(-2300/T)$	$Cl + H_2 \rightarrow H + HCl$
$d_7 = 1.8 \times 10^{-11} \exp(170/T)$	$Cl + HO_2 \rightarrow O_2 + HCl$
$d_{11} = 2.6 \times 10^{-12} \exp(-350/T)$	$HCl + OH \rightarrow H_2O + Cl$
$d_{32} = 2.9 \times 10^{-12} \exp(-800/T)$	$ClONO_2 + O(^3P) \rightarrow ClO + NO_3$
$d_{33} = 4.8 \times 10^{-13} \exp(700/T)$	$ClO + HO_2 \rightarrow HOCl + O_2$
$d_{34} = 3.0 \times 10^{-12} \exp(-500/T)$	$HOCl + OH \rightarrow H_2O + ClO$
$d_{35} = 1.0 \times 10^{-11} \exp(-2200/T)$	$HOCl + O \rightarrow OH + ClO$
$d_{50} = 5.0 \times 10^{-12} \exp(-1800/T)$	$CH_3CCl_3 + OH \rightarrow CH_2CCl_2 + HO_2$
$d_{61} = 5.0 \times 10^{-6} \exp(-8600/T)$	$Cl_2O_2 + M \rightarrow 2ClO + M$
$d_{62} = 4.5 \times 10^{-13} \exp(800/T)$	$OH + OClO \rightarrow O_2 + HOCl$
$d_{63} = 3.4 \times 10^{-11} \exp(160/T)$	$Cl + OClO \rightarrow 2ClO$
$d_{64} = 2.8 \times 10^{-11} \exp(-1200/T)$	$O(^3P) + OClO \rightarrow O_2 + ClO$
$d_{65} = 2.5 \times 10^{-12} \exp(-600/T)$	$NO + OClO \rightarrow NO_2 + ClO$
$d_{90} = 2.3 \times 10^{-10}$	$CFCl_3 + O(^1D) \rightarrow 3Cl +$ products
$d_{91} = 1.4 \times 10^{-10}$	$CFC_2Cl_2 + O(^1D) \rightarrow 2Cl +$ products

Table 1a. (continued)

Rate Coefficient, $cm^3\ s^{-1}$	Reaction
$e_{5a} = 6.7 \times 10^{-12}$	$ClO + BrO \rightarrow Br + OClO$
$e_{5b} = 2.9 \times 10^{-12} \exp(220/T) + 5.8 \times 10^{-13} \exp(170/T)$	$ClO + BrO \rightarrow Br + Cl + O_2$
$e_6 = 1.4 \times 10^{-12} \exp(150/T)$	$BrO + BrO \rightarrow Br + Br + O_2$
$k_1 = 4.2 \times 10^{-28}[M]/T^2$	$O(^3P) + O(^3P) + M \rightarrow O_2 + M$
$k_2 = 6.0 \times 10^{-34}[M](300/T)^{2.3}$	$O(^3P) + O_2 + M \rightarrow O_3 + M$
$k_3 = 8.0 \times 10^{-12} \exp(-2060/T)$	$O(^3P) + O_3 \rightarrow 2O_2$
$k_4 = 1.8 \times 10^{-11} \exp(110/T)$	$O(^1D) + N_2 \rightarrow O(^3P) + N_2$
$k_5 = 3.2 \times 10^{-11} \exp(70/T)$	$O(^1D) + O_2 \rightarrow O(^3P) + O_2$

Table 1b. Chemical Reactions Included in the Model

Reaction	κ_0^{300}	n	κ_∞^{300}	m	Reaction
b_{12}	2.2×10^{-30}	4.3	1.5×10^{-12}	0.5	$NO_3 + NO_2 + M \rightarrow N_2O_5 + M$
b_{22}	2.6×10^{-30}	3.2	2.4×10^{-11}	1.3	$NO_2 + OH + M \rightarrow HNO_3 + M$
b_{23}	1.8×10^{-31}	3.2	4.7×10^{-12}	1.4	$HO_2 + NO_2 + M \rightarrow HO_2NO_2 + M$
d_{31}	1.8×10^{-31}	3.4	1.5×10^{-11}	1.9	$NO_2 + ClO + M \rightarrow ClONO_2 + M$
d_{60}	1.8×10^{-32}	3.6	6.0×10^{-12}	0.0	$ClO + ClO + M \rightarrow Cl_2O_2 + M$

$$k = \frac{\kappa_0[M]}{1+\kappa_0[M]/\kappa_\infty} 0.6^{\{1+[\log_{10}(\kappa[M]/\kappa_\infty)]^2\}^{-1}} \qquad \kappa_0 = \kappa_0^{300}(T/300)^{-n} \qquad \kappa_\infty = \kappa_\infty^{300}(T/300)^{-m}$$

coupling between the chemistry and the model dynamics. In the "uncoupled mode" the chemistry can be run without influencing the dynamic simulation at all. In the "partially coupled" mode the water vapor distributions predicted by the MACCM2 and chemical sources of water vapor (primarily the methane oxidation) are coupled, but the ozone distributions are not. Dehydration can take place through the stratiform condensation parameterization of CCM2, where water vapor is removed to make supersaturated grid volumes just saturated. The prescribed ozone distribution is used for the radiative forcing. In the "fully coupled" mode both the ozone and the water vapor distributions are identical in both components. Solutions in the fully coupled mode will be described in a future paper.

This paper presents results from a 2-year run of the model in the "partially coupled" mode. Instantaneous values of the chemical species have been archived every two days over the 2-year integration. Initial conditions for the run were taken from the end of a 5-year run, in the uncoupled mode, used to bring the various species to near equilibrium. The chemical adjustment time for water vapor between 1 mbar and 100 mbar is between 250 and 3000 days [e.g., *Brasseur et al.*, 1990; *Mote* 1994], and the water vapor distribution is not yet fully equilibrated at the end of the simulation. Nevertheless, results for most species are reasonably representative of an equilibrated model.

Table 2. Photolytic Reactions in the Model

Reaction
$O_2 + h\nu \rightarrow O(^3P) + O(^3P)$
$O_3 + h\nu \rightarrow O(^3P) + O_2$
$O_3 + h\nu \rightarrow O(^1D) + O_2$
$H_2O + h\nu \rightarrow OH + H$
$H_2O_2 + h\nu \rightarrow 2OH$
$N_2O + h\nu \rightarrow N_2 + O(^1D)$
$CH_4 + h\nu \rightarrow CH_3 + H$
$NO_2 + h\nu \rightarrow NO + O(^3P)$
$HNO_3 + h\nu \rightarrow OH + NO_2$
$HOCl + h\nu \rightarrow Cl + OH$
$HO_2NO_2 + h\nu \rightarrow NO_2 + HO_2$
$ClONO_2 + h\nu \rightarrow NO_2 + ClO$
$N_2O_5 + h\nu \rightarrow NO_2 + NO_3$
$OClO + h\nu \rightarrow O + ClO$
$Cl_2O_2 + h\nu \rightarrow 2ClO$
$HCl + h\nu \rightarrow H + Cl$
$NO + h\nu \rightarrow N + O(^3P)$
$CO_2 + h\nu \rightarrow CO + O(^3P)$
$CH_3Cl + h\nu \rightarrow Cl +$ products
$CH_3CCl_3 + h\nu \rightarrow CH_3CCl_2 + Cl$
$CCl_4 + h\nu \rightarrow CCl_3 + Cl$
$CFCl_3 + h\nu \rightarrow 3Cl +$ products
$CFC_2Cl_2 + h\nu \rightarrow 2Cl +$ products
$NO_3 + h\nu \rightarrow NO_2 + O(^3P)$

4. Model Results

This section provides an overview of the general properties of the simulation of some of the species calculated in the model. The amount of information available for presentation can be overwhelming because of the many new dependent variables and simulation length. Therefore we restrict our discussion to a small subset of the spacescale and timescale features present and further restrict the discussion by only presenting results from 100 mb through 1 mb to focus on the area where the ozone distribution is a maximum. We hope to present other aspects of the simulation in future papers. Our presentation begins with distributions averaged over large scales in space and time and then focuses on features of smaller (time and spatial) scales.

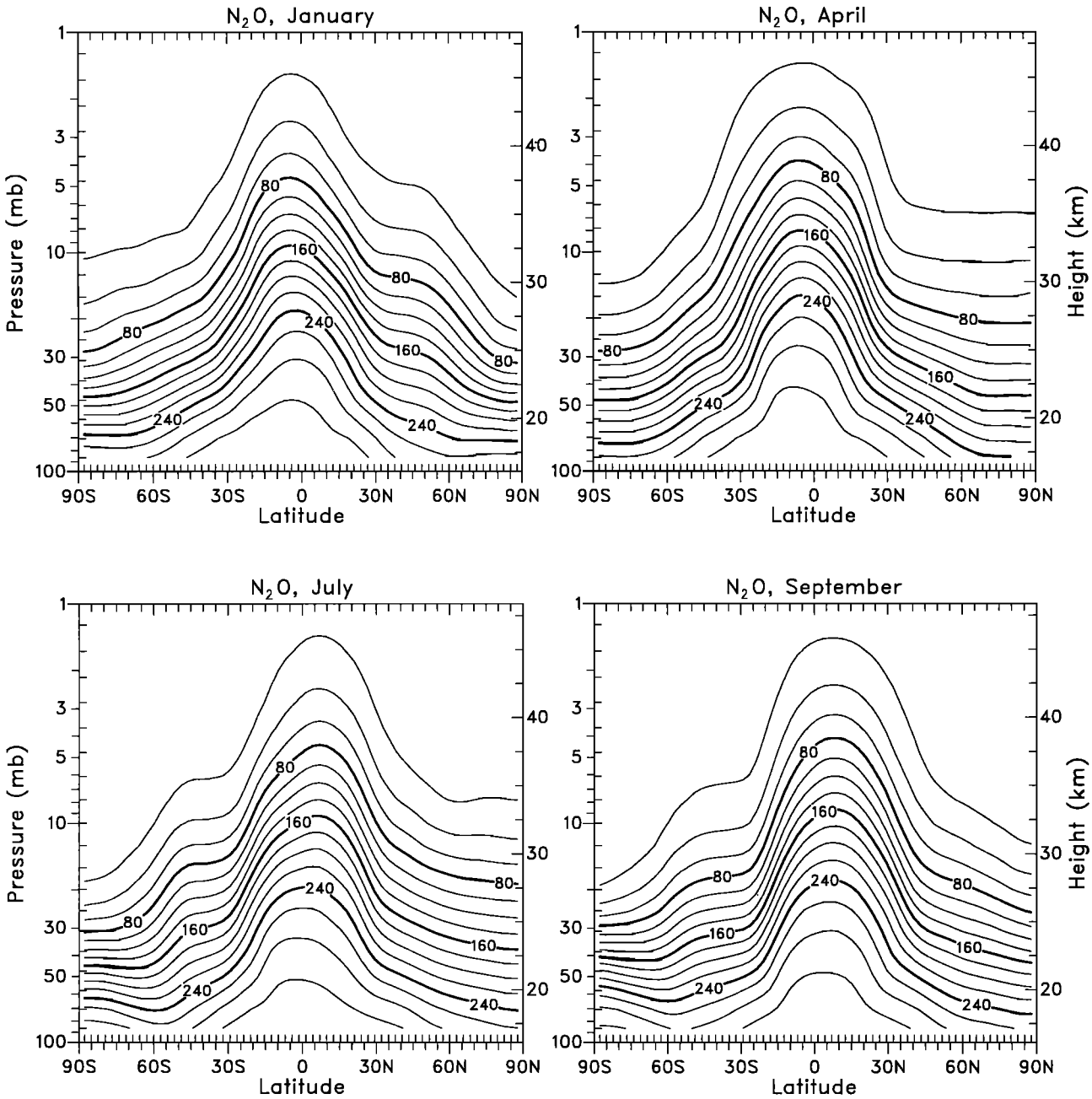

Figure 1. Model zonally averaged monthly mean values of N_2O. Contour interval is 20 ppbv.

4.1. N_2O, CH_4, and H_2O

These constituents have photochemical lifetimes that are long compared to the transport lifetime throughout most of the model domain. For this reason they serve as nearly inert tracers of dynamical motion and provide information regarding the transport circulation of the model.

Figure 1 shows the model zonally averaged monthly mean values for N_2O for the months of January, April, July, and October. Corresponding estimates for the atmosphere from the Stratospheric and Mesospheric Sounder (SAMS) instrument [*Jones and Pyle*, 1984] are provided in Figure 2. They may be contrasted to those presented by *Sassi et al.* [1993] and by *Randel et al.* [1994] who used a version of MACCM2 having much simpler, highly parameterized representations of the photolysis of N_2O. This gas is produced at the surface, mainly by complex nitrification and denitrification processes in soils. It acts as an inert tracer through the troposphere and the lower stratosphere and is destroyed by photolysis, or is oxidized, primarily above 20 km, providing an important source of stratospheric NO_x. The vertical distribution of N_2O between 1 mb and 30 mb corresponds qualitatively to the SAMS data. At altitudes below 30 mb the SAMS data are unreliable, due to potential overestimates of species abundance [*Jones and Pyle*, 1984]. The peak mixing ratio values are located near the equator and are indicative of relatively rapid upward transport through the tropopause. The

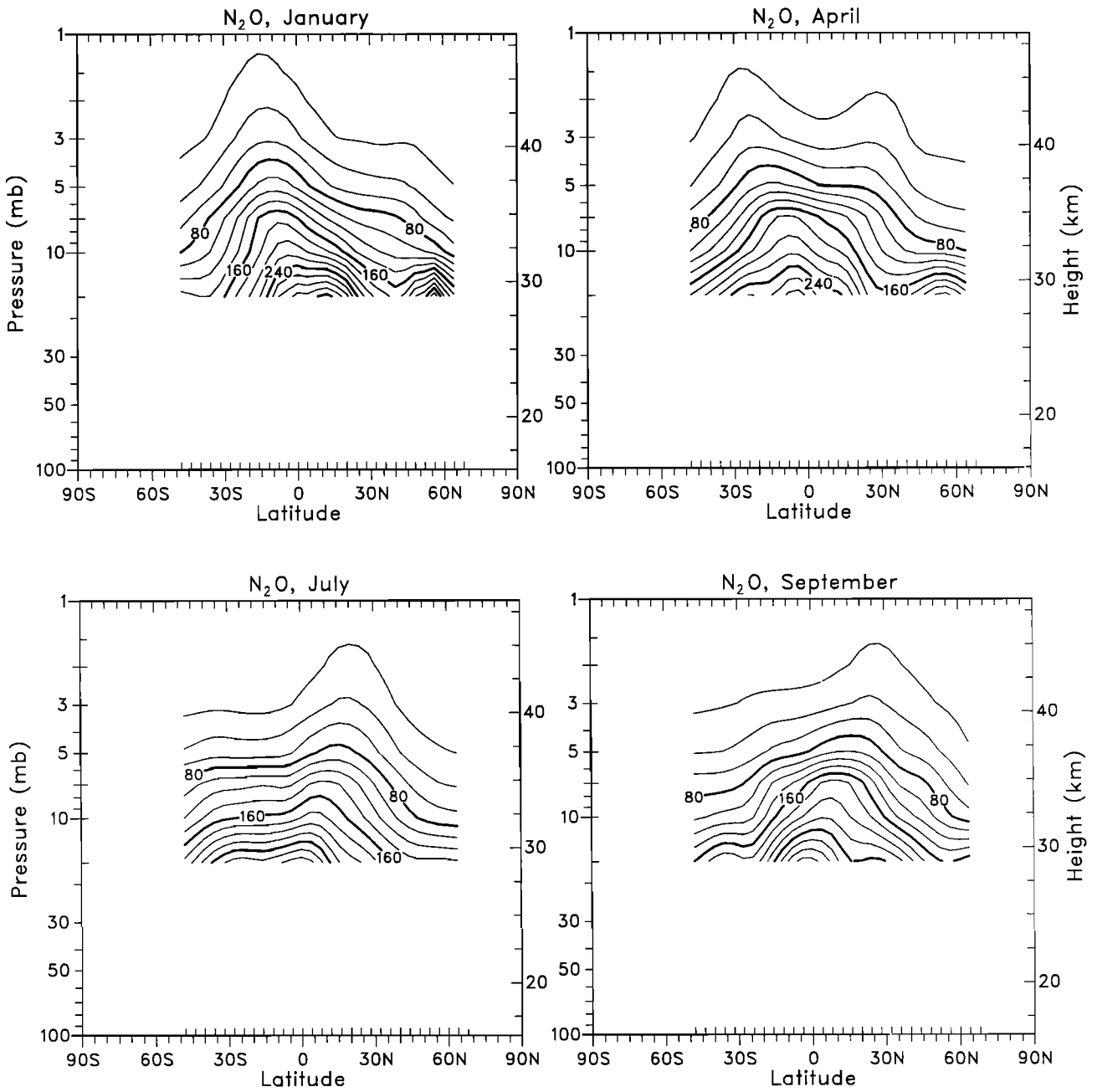

Figure 2. Stratospheric and Mesospheric Sounder (SAMS) zonally averaged monthly mean values of N_2O. Contour interval is 20 ppbv.

peak is not offset sufficiently toward the summer hemisphere, when compared to SAMS data, suggesting that the upward branch of the mean circulation is not sufficiently displaced. At 1 mb, equatorial values of N_2O with minimum values of around 10 ppmv are well simulated. The polar minima, indicative of subsidence, is also apparent. The flattening of the contours near 30° in the winter hemisphere, associated with mixing by planetary wave breaking [*Garcia*, 1991], is present in the model. The very sharp gradients separating the tropics and extratropics and the secondary maxima in the gradients, separating the midlatitudes from the polar region in the winter hemisphere, are also seen. The asymmetry between northern and southern hemisphere winters is evident, with northern hemisphere features located closer to the pole and the polar minima at lower altitudes in the southern hemisphere winter. These features are due to the larger planetary wave activity present in the northern hemisphere, which acts to mix more rapidly in the northern hemisphere.

Unfortunately, there is no evidence in the model solutions for the "double-peak" structure in the upper stratosphere during the equinox months, seen in the SAMS data and thought to be one manifestation of the Semi-Annual Oscillation (SAO). This is consistent with our earlier observation that the SAO westerly phase is

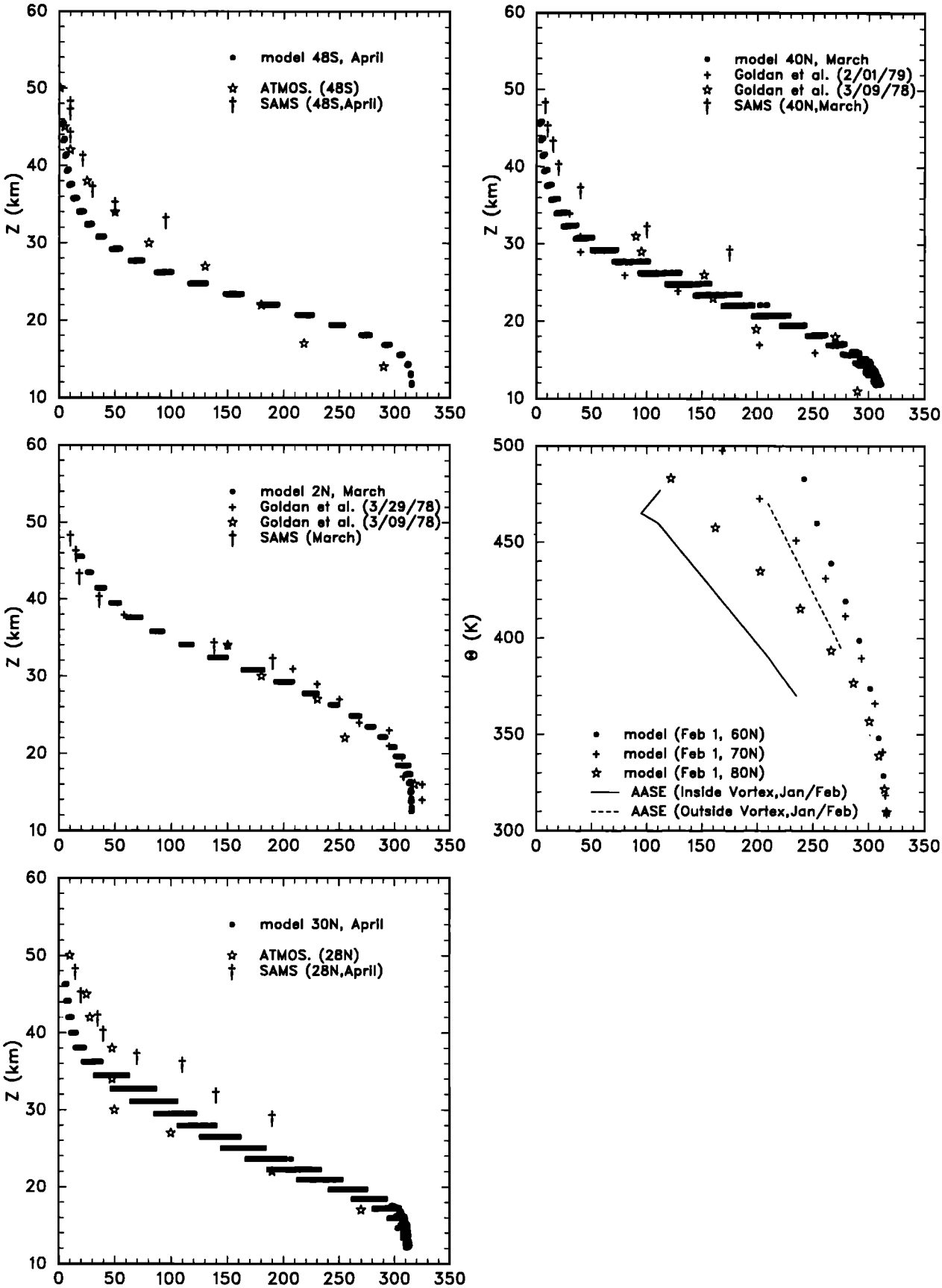

Figure 3. (top left) Vertical profiles of N_2O at 48°S, (middle left) 2°N, (bottom left) 30°N, (top right) 40°N, and (middle right) north polar latitudes. The solid and dashed lines in the polar region panel represent approximate lines of best fit to the data as taken from *Podolske et al.* [1989].

too weak in the model. Although stronger than that seen in the SAMS data, the pole-to-equator gradient of N_2O is probably too small (compared to other observations) in the lower stratosphere. This and other features can be seen more easily in vertical profiles of N_2O (Figure 3) taken from a variety of sources. The tropical soundings match observations closely. As in the study of *Garcia et al.* [1992], the data from *Goldan et al.*, [1980, 1981] have been divided by 1.07 to correct for systematic measurement errors, and SAMS data have been displayed only above 30 km. The model results represent the monthly averaged values at each grid point between 10 and 50 km and thus provide an estimate of the variation of N_2O along a latitude circle. The agreement in the tropics is quite good, even above 35 km, where *Garcia et al.* [1992] found substantial overestimates in their model results. The lack of spread in the model values (indicated by the clustering of the black dots) suggests very little longitudinal variability. In the subtropics (30°N) the spread in model values is much larger, and profiles tend to lie between those of the Atmospheric Trace Molecule Spectroscopy (ATMOS) experiment and SAMS, which differ markedly from each other in the 30- to 38-km altitude range. At 40°N the model spread is quite large, and the values lie nearer to the Goldan profiles, than those of SAMS. At 48°S the model shows a stronger vertical gradient than the observations. Polar profiles from early February along a meridional cross section in the model are compared with averaged profiles taken from the Airborne Arctic Stratospheric Expedition (AASE) flights during January/February [*Podolske et al.*, 1989]. The strong

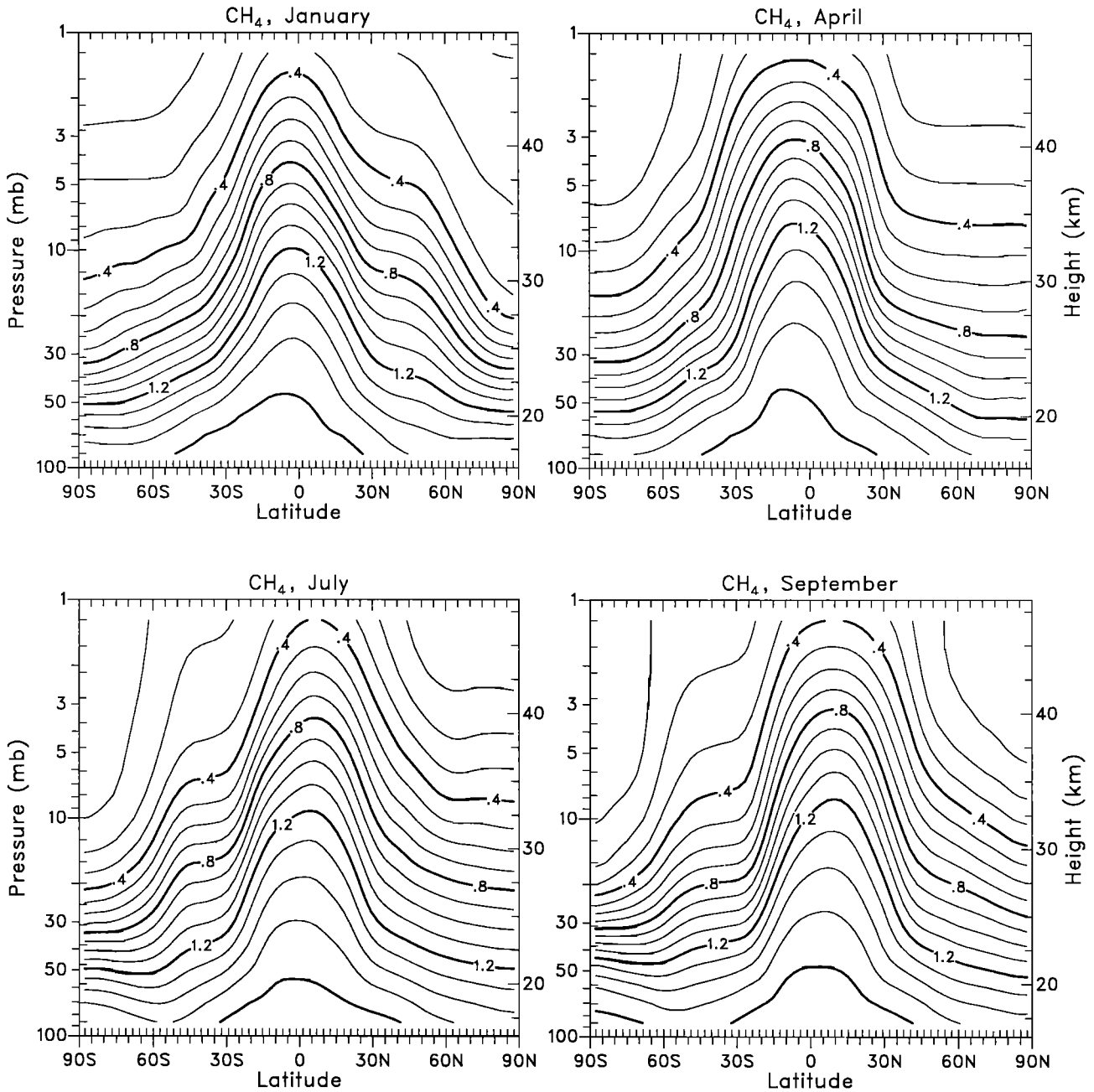

Figure 4. Model zonally averaged monthly mean values of CH_4. Contour interval is 0.1 ppmv.

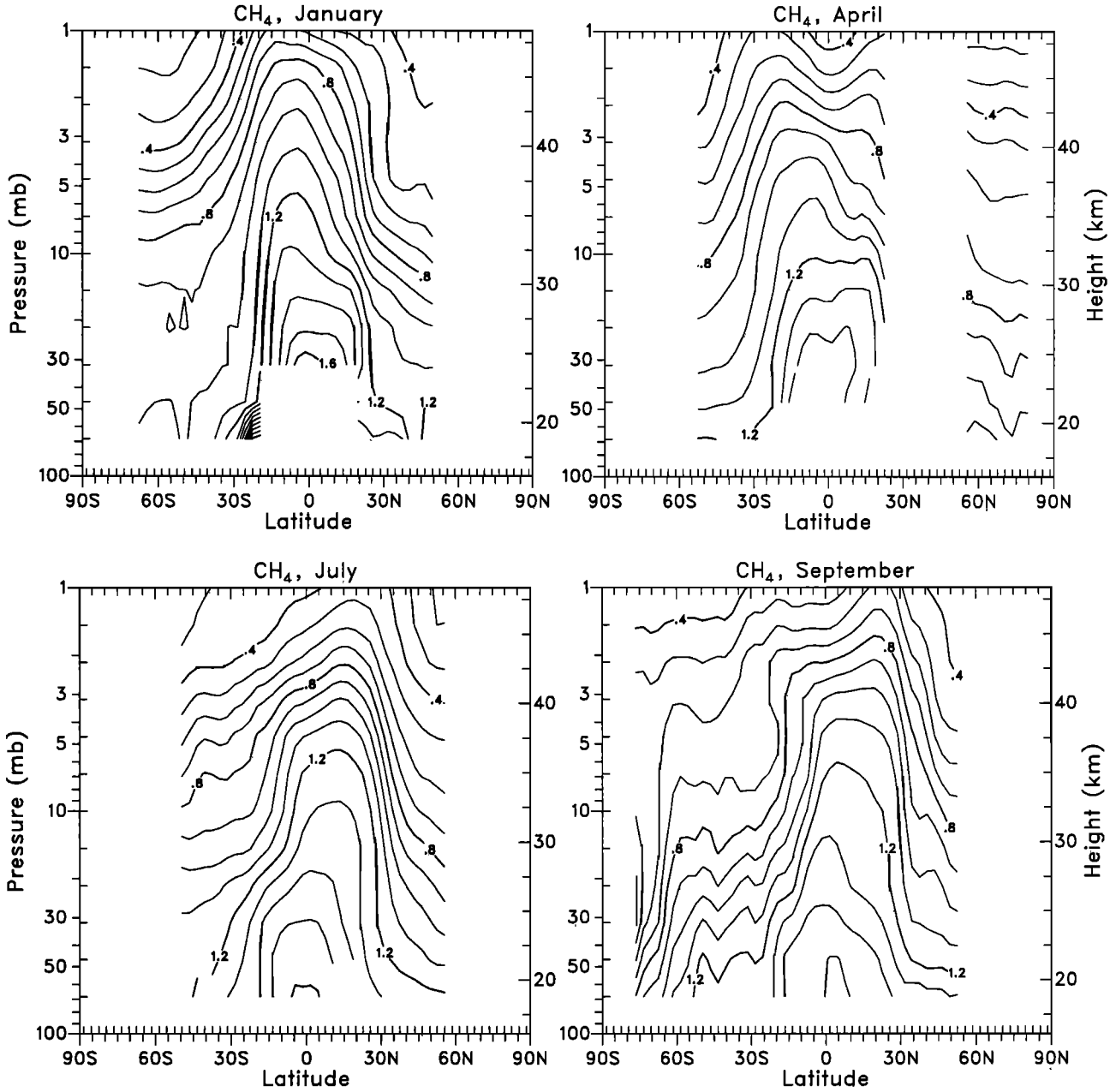

Figure 5. Halogen Occultation Experiment (HALOE) zonally averaged monthly mean values of CH_4. Contour interval is 0.1 ppmv.

gradients characteristic of the polar vortex edge are apparent, although the model values are not sufficiently low in the lower stratosphere. It is interesting to contrast the model results to the Cryogenic Array Etalon Spectrometer (CLAES) distributions shown by *Randel et al.* [1994]. The model results are very much closer to CLAES data than to the corresponding SAMS data, which shows a stronger double-peaked structure during the equinox, generally higher values of N_2O, and the peak more offset toward the summer hemisphere than the CLAES data.

The zonally averaged distributions for methane are shown in Figures 4 (model) and 5 (observations). (Note that The observations represent version 16 data from the Halogen Occultation Experiment (HALOE) instrument [*Russell et al.*, 1993]. Figure 5 was constructed by binning the data into latitude height boxes, then averaging whatever data were in that bin. Data with values greater than 2 ppmv, or where the data quality flag was more than 10% of the data value, were excluded, as was that below 70 mb. After the averaging operation, the data were smoothed with a 1/4, 1/2, 1/4 weighted filter in latitude. Contours stop at bins where there were no data.) Methane is also a relatively long-lived species in the middle atmosphere, but its profile is controlled more strongly by photochemistry. The same structures seen in N_2O are present in CH_4. Model values are somewhat too low at 1 mb (about 50 km) when compared to the

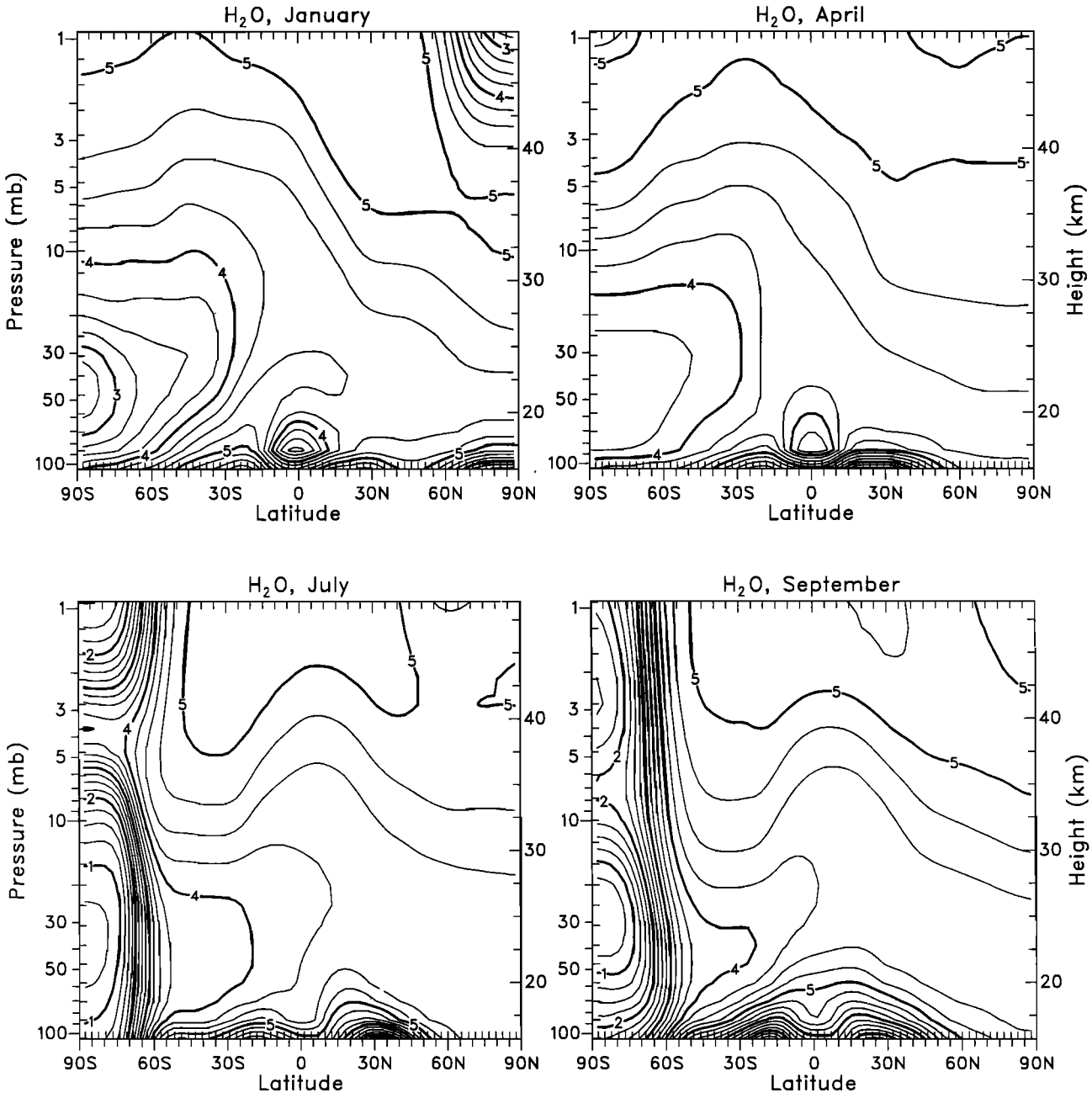

Figure 6. Model zonally averaged monthly mean values of H_2O. Contour interval is 0.25 ppmv.

SAMS or HALOE data. The model contours between 1 and 10 mb are shifted downward about one level (2-3 km) when compared to those of the observations. It is not clear whether this discrepancy is due to numerical issues and resolution or to problems with the meridional circulation itself. A notable discrepancy with observation occurs within the Antarctic vortex in winter and spring, where the HALOE observations show uniformly low values of methane between about 2 and 30 mb. This region extends only to 10 mb in the model and suggests that there is not sufficient descent within the polar vortex. *Garcia and Boville* [1994] showed that the weakness of the descent within the vortex is the principal cause of the low polar temperatures noted earlier and is related to insufficient gravity wave momentum flux.

Monthly mean zonal averages for H_2O are shown in Figure 6 for the model version that includes the methane oxidation mechanism as a source for model water vapor. Lower- and middle-stratosphere values have not yet equilibrated; the H_2O distribution is still adjusting to the methane oxidation source, although addition of this term has improved the distribution of water vapor substantially in the upper stratosphere and lower mesosphere, increasing the zonally averaged values there from less than 1-2.5 ppmv to 4-6 ppmv (E. W. Chiou, et al., Proposed reference model for middle atmosphere water vapor, submitted to *Advances in Space Research*, 1994, hereinafter referred to as C94). The

minimum associated with dehydration near the tropical tropopause shows a seasonal cycle, which is strongest during northern hemisphere winter, consistent with enhanced mean upward motion and lower temperatures occurring when the planetary wave activity is at a maximum [*Yulaeva et al.*, 1994]. The region of dehydration in the southern pole in spring is too deep, extending as high as 20 mb, and the values within it are somewhat too low, reflecting the much too cold temperatures present there and the overly strong and persistent polar vortex. The very low mixing ratios at the winter pole above 3mb are caused by descent of air from the mesosphere where the H_2O has been photolyzed. This H_2O minimum is not found in the results of *Mote et al.* [1993] using parameterized chemistry. The signature between 35 and 50 km is generally correct when compared to a proposed reference model for middle atmospheric water vapor [C94] that attempts to composite data from different satellite instruments (SAGE, SAMS, Limb Infrared Monitor of the Stratosphere (LIMS), and ATMOS). For example, during January the model shows highest values in southern hemisphere extratropical latitudes, with a minimum between 30°S and the equator, a secondary maximum in northern hemisphere midlatitudes, and a minimum over the northern hemisphere polar region. The model southern hemisphere maximum is somewhat too low (5.0 ppmv) when compared to the reference (5.5 ppmv). The reference shows a very strong

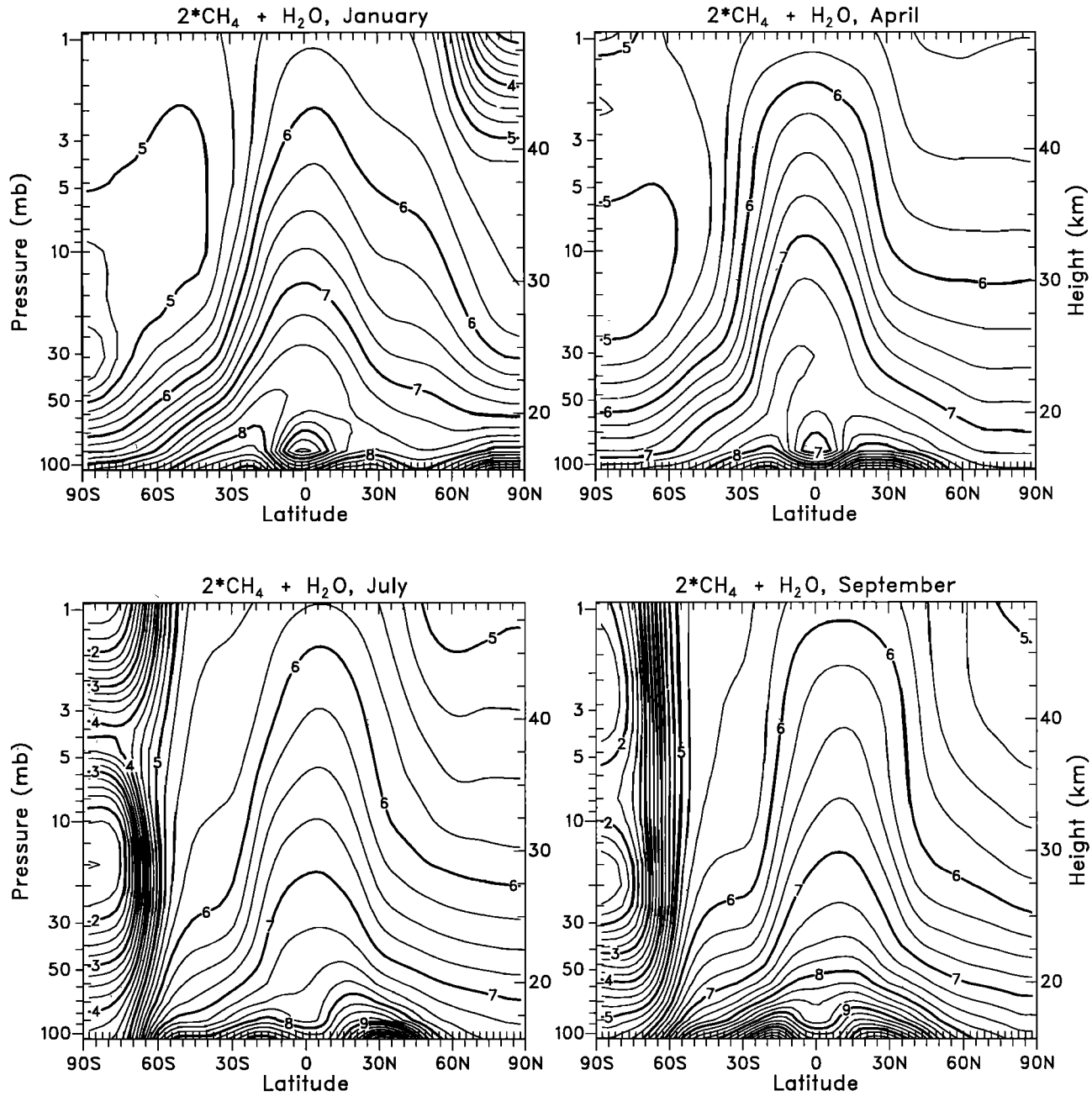

Figure 7. Model zonally averaged monthly mean values of $2CH_4 + H_2O$. Contour interval is 0.25 ppmv.

gradient at 60°N associated with the descent of air with low values of H_2O from the mesosphere. There is a corresponding gradient in the model, but it is weaker and too far poleward. The low region of water vapor has not descended deeply enough, and its latitudinal extent is not large enough. This problem is similar to that seen in state-of-the-art, two-dimensional models, [e.g., *Garcia and Solomon*, 1994].

Since the primary chemical source of H_2O in the middle atmosphere is the oxidation of methane, the sum $2CH_4 + H_2O$ is approximately conserved away from other sources and sinks [*Le Texier et al.*, 1988]. Deviations from a uniform distribution provide an indication of regional dehydration and transport from the troposphere. This field shows more stratification than is shown in the atmosphere (Figure 7), additional evidence suggesting that the model has not yet equilibrated. The model shows an extreme version of the dehydration over the pole seen during southern hemisphere winter. The upper stratospheric minimum results from mesospheric dehydration and is not seen in the results of *Mote et al.* [1993], while the lower stratospheric minimum results from the excessively low temperature simulated there.

4.2. O_3, NO_y and Cl_x Species

Monthly mean zonal averages for the model ozone distribution are shown in Figure 8. Appearing in Figure 9 are the corresponding values from a data set constructed by combining data from the Solar Backscatter

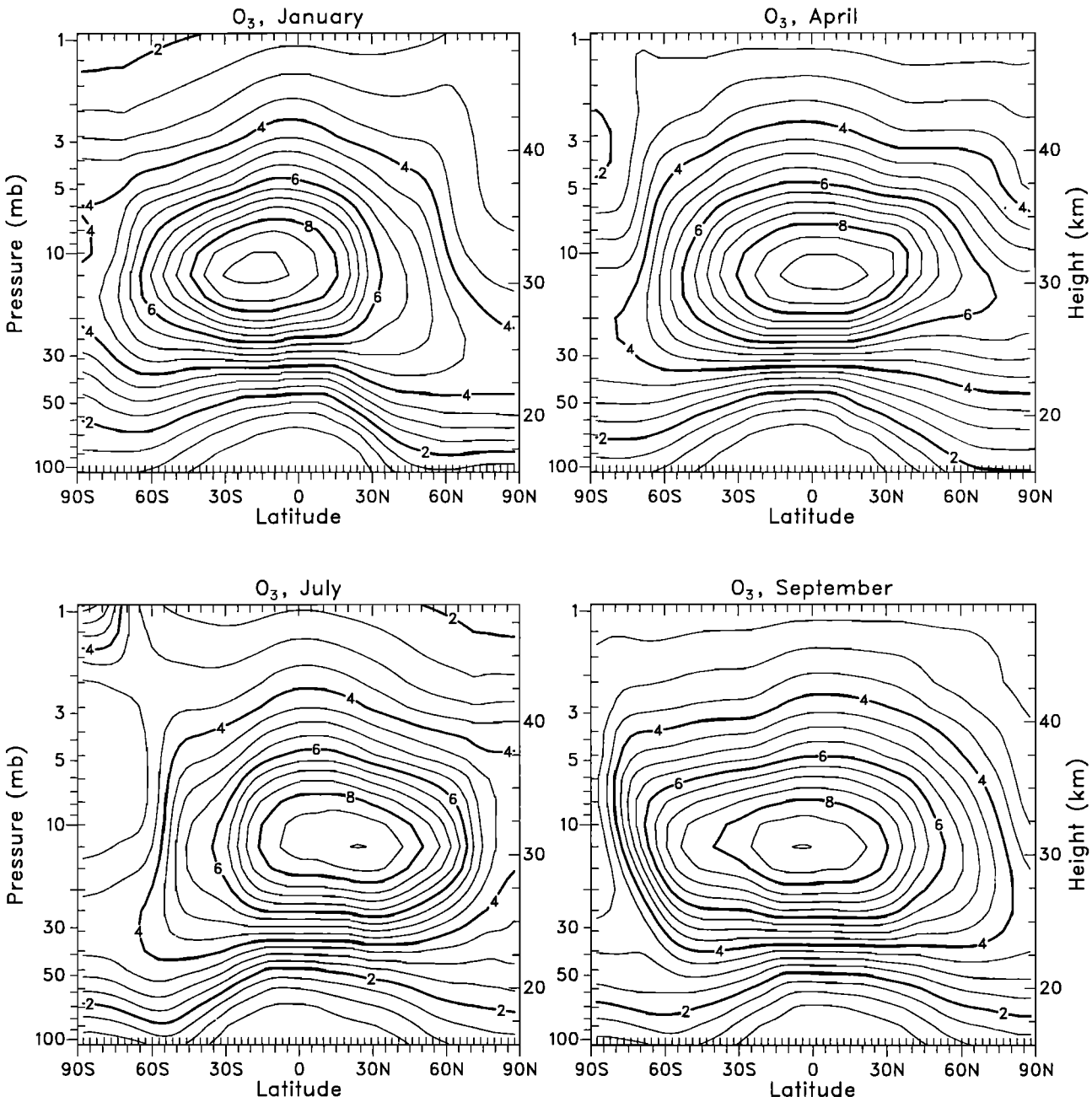

Figure 8. Model zonally averaged monthly mean values of O_3. Contour interval is 0.5 ppmv.

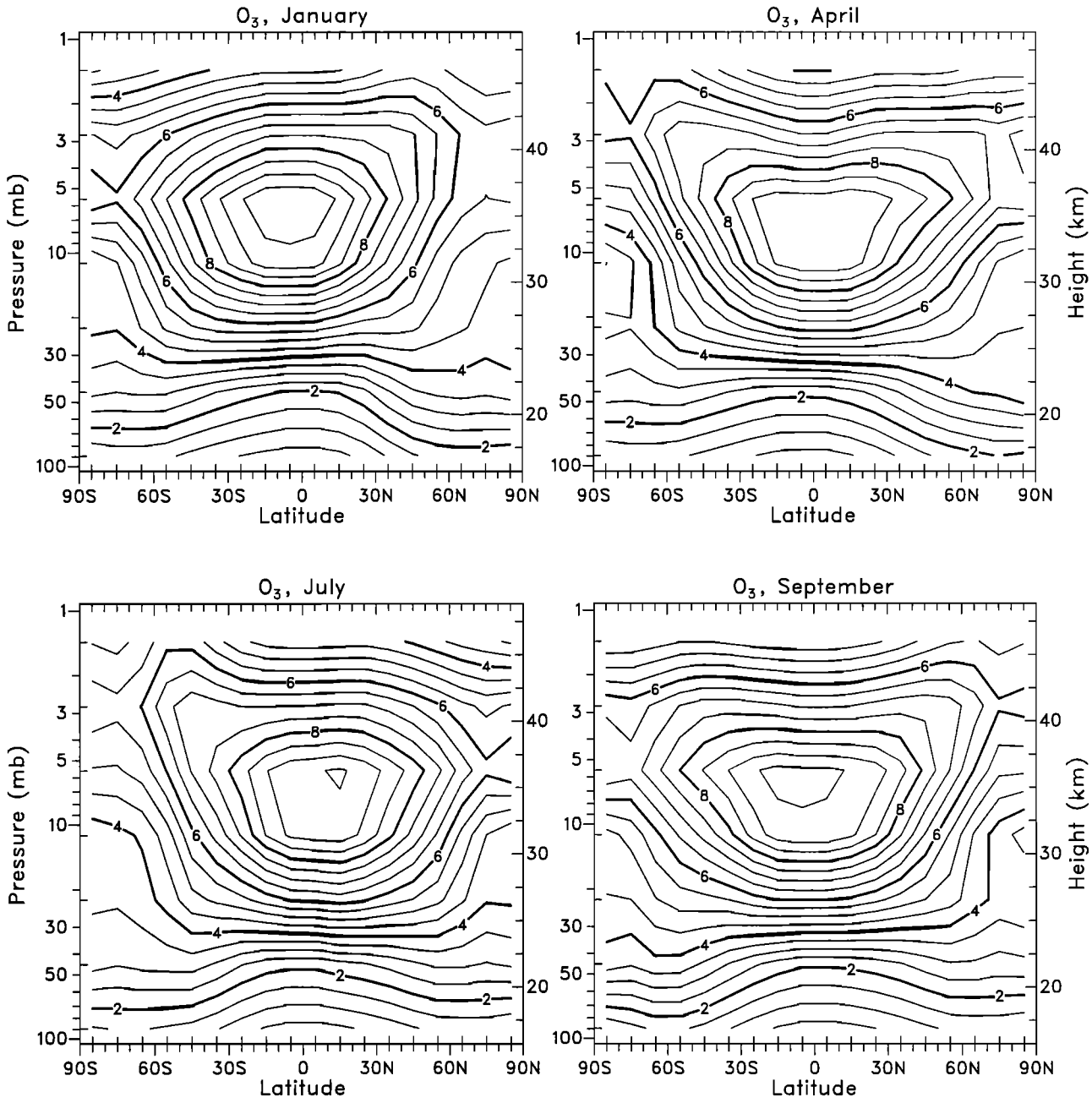

Figure 9. Data zonally averaged monthly mean values of O_3. Contour interval is 0.5 ppmv.

Ultraviolet (SBUV) and SME for the late 1970s and early 1980s. Many features of the observed distribution can be found in the model. The equatorial peak of about 9 ppmv is slightly smaller than that seen in the observations and appears at too low an altitude (9 to 20 mb in the model, 5 to 10 mb in the observations). The observations show a characteristic "banana" shape in the meridional ozone distribution during January and July, with the ozone maxima ascending as one moves poleward. At the poles the maximum values in mixing ratio occur at about 40 km in the observations. The maximum occurs at a higher altitude at the winter pole than at the summer pole. In the polar night the observations show a slight reduction of the height of the maximum as a result of downward transport by the residual mean circulation. These characteristic features are somewhat different in the model simulation. The vertical maximum is aligned much more horizontally through the subtropics than in the observations. The model polar maximum is much lower than seen in the observations. This is also apparent in the profiles (Figure 10), where values from the model and observations may be more easily compared. We have not yet been able to identify whether our inability to model this feature of the O_3 distribution is due to problems in the chemistry or the transport circulation. Another defect of the simulation is the underestimate of ozone abundance at 40 km (3 mb), a characteristic

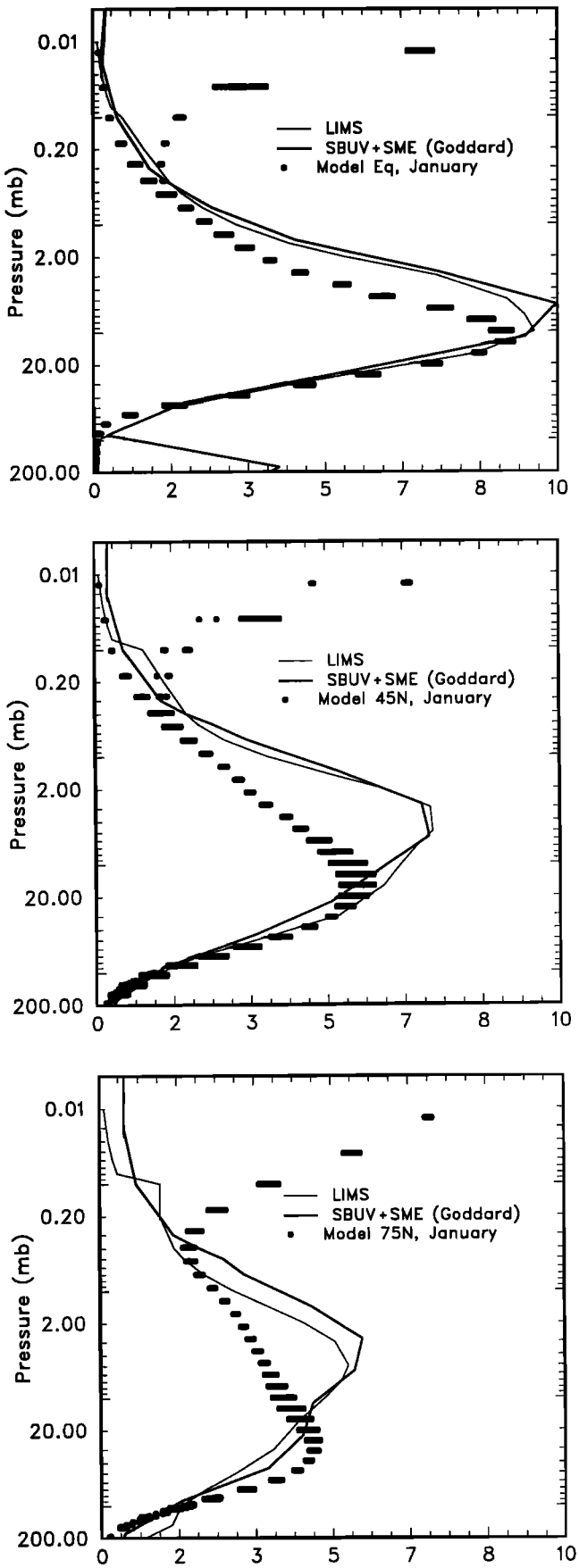

Figure 10. Vertical profiles of O_3 at (top) 2°N, (middle) 45°N, and (bottom) 75°N.

seen in virtually all models of ozone chemistry [*WMO*, 1985; *Eluszkiewicz and Allen*, 1993]. This "ozone deficit problem" remains an open question, and current speculations center on a chemical, rather than a dynamical explanation, because of the short photochemical timescales. In our model the problem is made worse by excessively high values of Cl_x (from the CFC source terms adopted in the model). Our values of ClO in the upper stratosphere are approximately 30 % higher than the concentrations found in various 2-D models [*WMO*, 1985], but a factor of 2 higher than the observation at 30°N by *Stachnik et al.* [1992]. Also, including the reaction $ClO + OH \rightarrow HO_2 + Cl$ might somewhat improve the simulation. Above 0.2 mb there are also substantial differences between model and observations (which represent only daytime values). In the model, one can see points clustering about two lines. The line with lower values near to the observations are characteristic of daytime values of O_3 in which much of the O_x family resides in the oxygen atoms. During the night these atoms return to O_3 and substantially augment the O_3 daytime values.

The zonal average of the column-integrated ozone as a function of latitude and time (Figure 11) has many realistic features. Peak values in the northern hemisphere occur during March and April at 70°-80°N, following the breakdown of the polar vortex, reaching a maximum of about 420 Dobson units (DU), followed by a minimum in September. The tropical minimum of approximately 270 DU shows approximately the right seasonal migration across the equator. The low values in the 3-D model occur during December to March and are suggestive of a vigorous tropical upwelling driven by the stronger planetary wave activity in the northern hemisphere winter. In the southern hemisphere the midlatitude spring maximum is evident, although the model values are 15% too low. The breakdown of the polar vortex in late October and migration of the ozone maximum to the pole is missing in the model, which maintains unrealistically low ozone amounts throughout the year. The ozone distribution is reminiscent of a perpetual ozone hole, despite the fact that we have not included the relevant heterogeneous chemistry in the simulation. This field in particular, as well as the distributions of N_2O, CH_4, and H_2O are manifestations of substantial problems in the model circulation in the southern hemisphere, associated with the inadequacy of the gravity wave parameterization in the southern hemisphere. As seen in the work of *Boville* [this issue], this is because the polar vortex structure is far too strong in the simulation, maintaining a strong barrier to transport year round. The "pseudo ozone hole," seen in the simulation, therefore exists for the wrong reason. We thus focus primarily on the northern hemisphere circulation in the following paragraphs and return to a discussion of the problems in the southern hemisphere extratropics in the summary.

Maps of the monthly mean ozone column abundance are shown in Figure 12. Note the distinct maxima in midlatitudes corresponding to the positions of station-

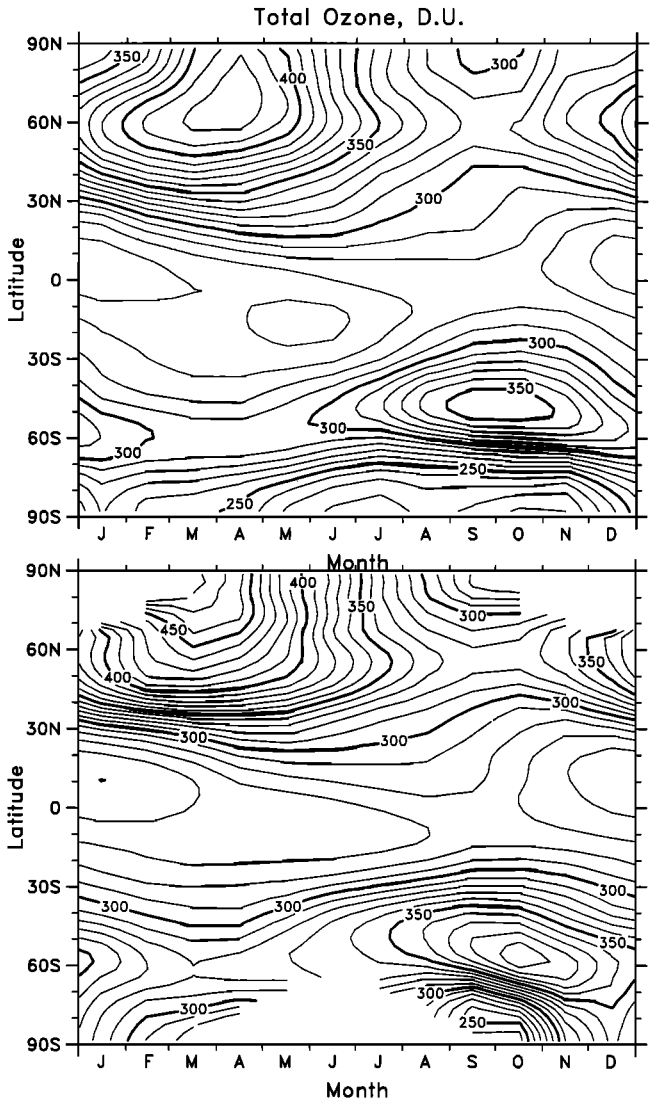

Figure 11. Latitude time contours of the zonally averaged, monthly averaged column-integrated O_3 in Dobson units (DU) for (top) a 5-year ensemble average of the model, and (bottom) from the Total Ozone Mapping Spectromer (TOMS) instrument (1979-1984).

ary planetary wave troughs, which migrate appropriately with season. Minima are seen over regions of deep convection. Very low values of ozone are pervasive over the Antarctic continent, with lowest values occurring during October, just prior to the breakdown of the southern hemisphere polar vortex.

As the major loss process for ozone in the stratosphere is provided by nitrogen oxides, it is important that the nitrogen family be treated in detail. For the sake of illustration, results representative of the month of January will now be presented and discussed. Figure 13 shows the zonally averaged mixing ratio of odd nitrogen ($NO_y = N + NO + NO_2 + NO_3 + 2N_2O_5 + HNO_3 + HNO_4 + ClONO_2$) as a function of latitude and altitude. Since NO_y can be considered as a long-lived tracer in the stratosphere, this distribution is strongly influenced by the general circulation. It is produced primarily through the oxidation of N_2O, then transported poleward and downward. In the region of production (the tropics) the mixing ratio of NO_y reaches approximately 20 ppbv. The meridional transport is strongest during winter, when planetary wave activity is most intense. This is particularly evident in January when a secondary maximum is produced in the polar region of the northern hemisphere between 22 and 26 km altitude.

The distribution of NO_y in the lower stratosphere is directly influenced by the variation with latitude of the tropopause height and the rapid loss of NO_y in the troposphere by washout and rainout processes. Low mixing ratios in the tropical lower stratosphere are directly related to the strong upwelling in this region, while the relatively high values poleward of 60° latitude are caused by downward transport in these regions. It should be stressed that the existence of strong vertical gradients in the mixing ratio of NO_y, in layers where dynamical processes at synoptic scale seem to play an important role, should influence dramatically the budget of odd nitrogen. A correct description of the behavior of nitrogen compounds in the lower stratosphere and upper troposphere can only be achieved by three-dimensional models at the high spatial and temporal resolution.

The distribution of NO_y in the upper stratosphere, especially at high altitude, is directly influenced by dynamical exchanges with the mesosphere and even the thermosphere, especially in the winter high-latitude regions [e.g. *Solomon, et al.*, 1982]. As the mesosphere acts as a sink for NO_y (through NO photolysis and recombination between N and NO), low mixing ratios of NO_y are predicted by the model in these regions, despite intense downward transport. If the model extended to the lower thermosphere, where odd nitrogen is produced as a result of ionic processes, downward transport from the thermosphere would tend to produce a maximum (rather than a minimum) in the mixing ratio of NO_y in the polar winter and bring the calculated values more in line with observations [*Russell et al.*, 1988]. The results with the current model configuration suggest that the influence of processes occurring above the stratopause reaches levels as low as 30 km altitude in the polar region during winter.

The bottom panels of Figure 13 compare NO_y profiles derived from ATMOS data [*Russell et al.*, 1988] at 48°S and 30°N with model results. The model profiles show peak values at lower altitudes than seen in the observations, consistent with other long-lived species discussed previously. The apparent overestimation of NO_y below 35 km altitude (and, consequently, the overestimation of NO_x) leads to higher values of ozone destruction than might otherwise be expected. The problem is more complex when heterogeneous chemistry is included.

The zonally averaged distributions of individual members of the nitrogen family sampled are shown in Figure 14. In the case of NO the zonally averaged mixing ratio increases with height and reaches a maximum of 8.5 ppbv at 45 km over the equator and 9.5 ppbv at

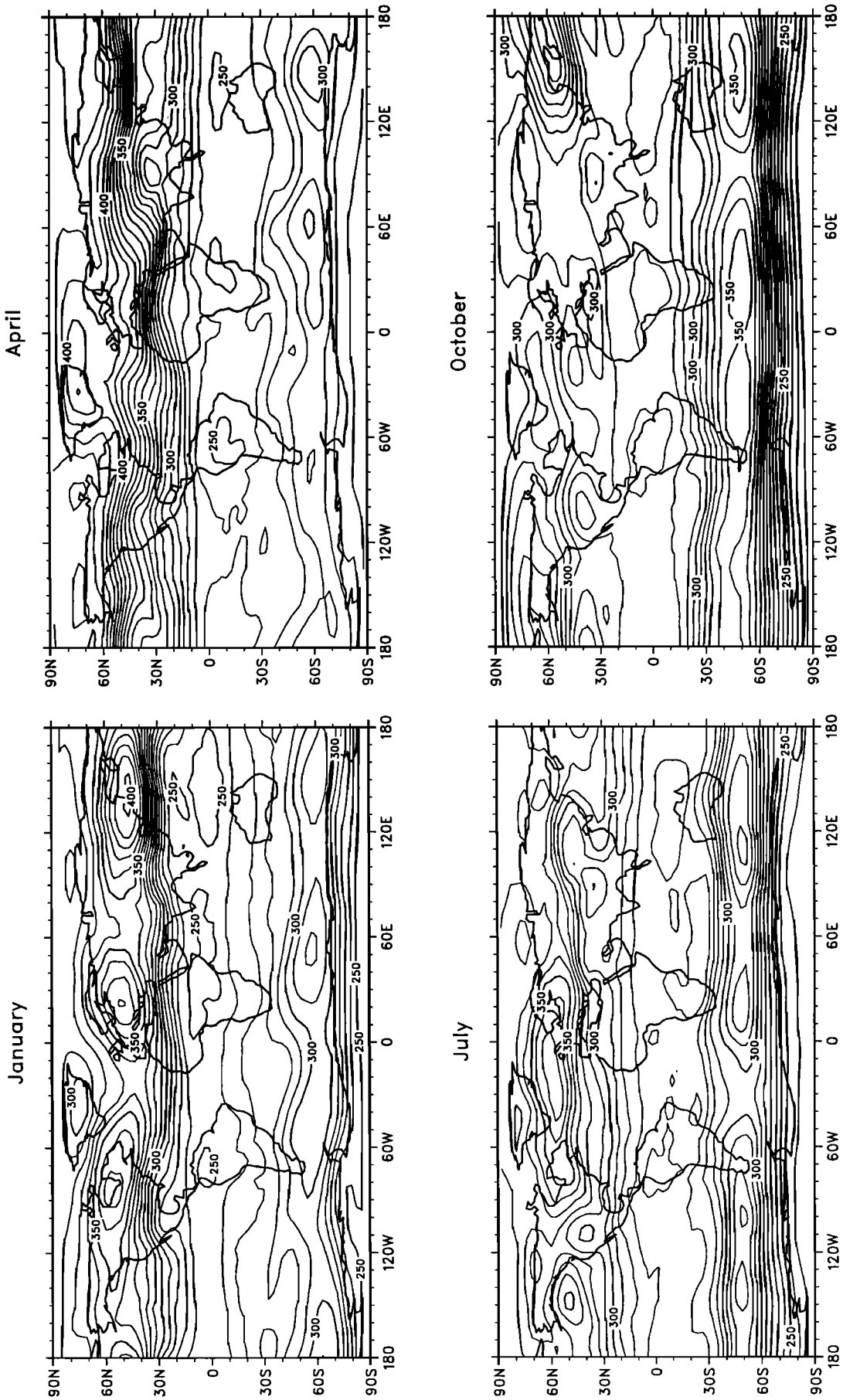

Figure 12. Monthly mean column ozone abundance as a function of latitude and longitude. Contour interval is 10 DU.

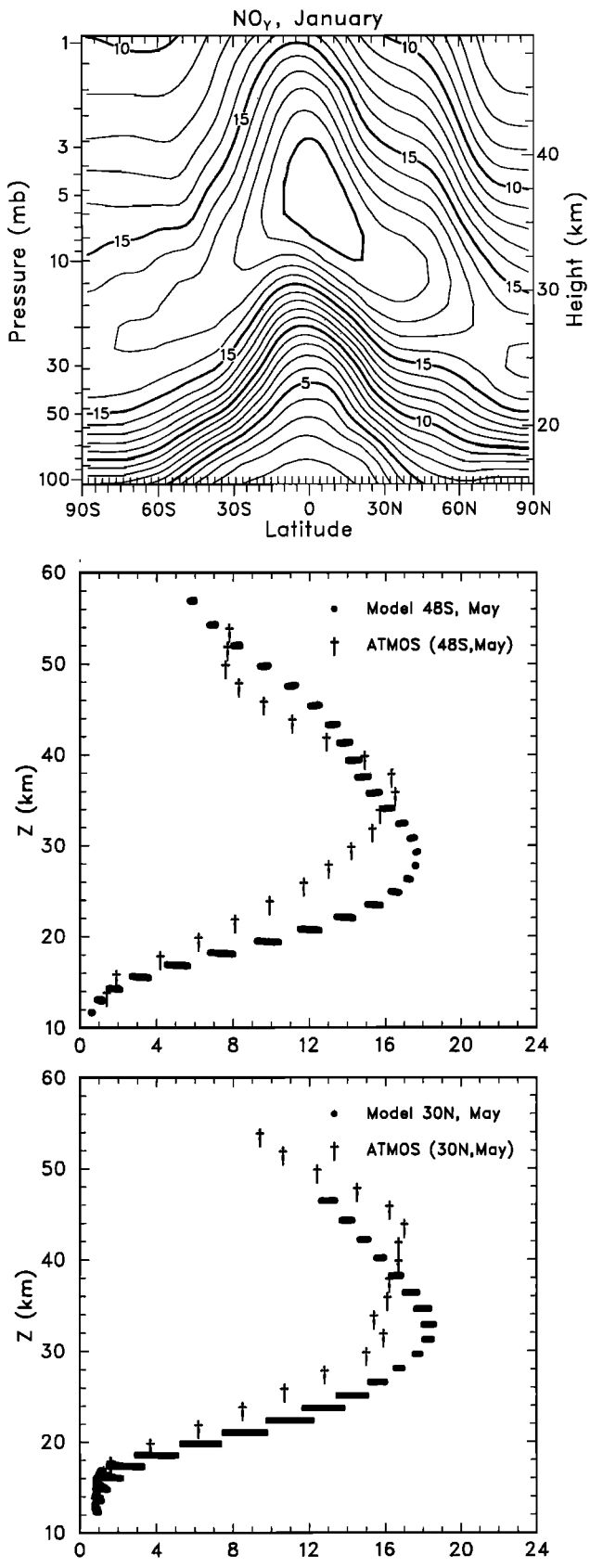

Figure 13. NO_y distributions for the model and some observations (top) Zonal average, monthly averaged January distribution. Contour interval is 1 ppbv; (middle) profiles at 48°S. (bottom) Profiles at 30°N compared to SAMS.

the same height in the polar region during the summer (polar day). Mixing ratios are low in the winter hemisphere, especially at low altitude, since NO is entirely converted into other nitrogen compounds in the polar night. The distribution of NO_2 is characterized by a maximum in the zonally averaged mixing ratio, which reaches 11 ppbv at 38–40 km over the equator. In the case of NO but to a lesser extent than NO_2, there is a clear lack of symmetry between the summer and the winter hemispheres. In both cases the mixing ratio (e.g., at 30 km altitude) is highest in the summer hemisphere. This pattern results from the conversion of NO_2 into N_2O_5 which is most efficient in winter and at high-latitudes, when the photodecomposition of N_2O_5 is slow. Figure 14 (bottom left) shows that N_2O_5 (a source of NO_2 and NO_3) is most abundant in the polar region of the winter hemisphere where it sequesters a substantial fraction of the odd nitrogen.

Finally, the zonally averaged distribution of nitric acid is shown in Figure 14 (bottom right). Because HNO_3 is the most abundant odd nitrogen compound in the lower stratosphere, its distribution is very similar to that of NO_y, where its mixing ratio increases with latitude, typically from 2 ppbv at the equator to more than 7.5 ppbv at the pole. Above 25 km altitude, its mixing ratio decreases with height because the formation of HNO_3 by $NO_2 + OH$ is pressure dependent, and the photolysis of HNO_3 becomes efficient. It should be noted that the magnitude of the HNO_3 maximum mixing ratio in the polar lower stratosphere during winter (8.5 ppbv) is substantially lower than the values commonly observed (15 ppbv). The discrepancy is again attributed to the fact that in its present version the model ignores the heterogeneous reactions that convert N_2O_5 into HNO_3 on the surface of sulfate aerosols and ice particles in polar stratospheric clouds. The existence of a minimum in the HNO_3 mixing ratio in the polar night above 25 km altitude (as opposed to a maximum as seen in the LIMS data) is suggestive of downward transport of HNO_3 poor air and the lack of local heterogeneous production of nitric acid on very small quantities of aerosol particles [*Garcia and Solomon*, 1994].

N_2O_5 is notoriously difficult to measure directly. A comparison of our profile of N_2O_5 with a "pseudo" observation, which used ATMOS data to rescale a model profile [*Toon et al.*, 1986], is shown in Figure 15, with the accompanying HNO_3 profile. If the *Toon et al.* [1986] profile is correct, then it suggests a substantial overestimate of N_2O_5 below 30 km by the model and an underestimate above that level. Agreement below 30 km would be substantially improved by including the effects of the reaction of $N_2O_5 + H_2O$ on a background level of sulfate aerosols.

The treatment of chlorine compounds in the model is relatively simple. As mentioned earlier, because the complete series of chlorofluorocarbons is not included in the chemical scheme, we scaled CFC-11 and CFC-12 so that the load of inorganic chlorine reaches approximately 4 ppbv (a slightly higher value than currently observed) above 30 km altitude. In addition, because

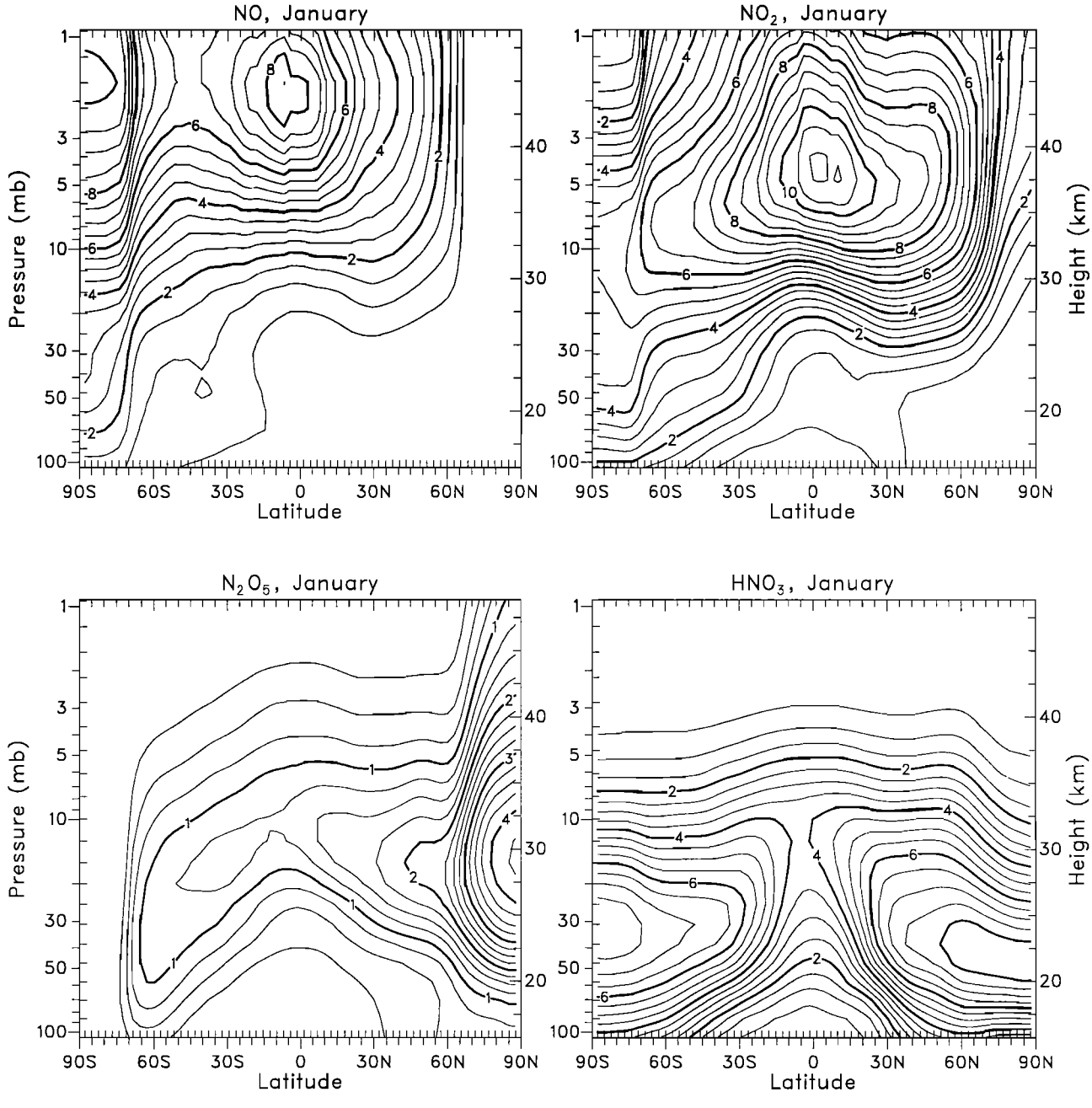

Figure 14. January zonal averages of some members of the NO_y family in ppbv: (top) NO, (top) NO_2, (bottom) N_2O_5, and (bottom right) HNO_3.

we have deliberately ignored the effect of heterogeneous reactions on the surface of solid and liquid particles, the high ClO mixing ratios observed in the polar region during winter and spring should not be reproduced.

Figure 16 presents the zonally averaged concentrations of ClO, $ClONO_2$, HCl, and HOCl. Consistent with observations (in air unprocessed by PSCs), the mixing ratio of ClO reaches maxima slightly higher than 1 ppbv in the polar upper stratosphere during winter. Chlorine nitrate concentrations are largest between 25 and 30 km altitudes with maxima at high latitudes in winter. Note that in this region, $ClONO_2$ sequesters more than 2 ppbv of odd nitrogen, so that it affects significantly the budget of NO_y in the lower stratosphere. The mixing ratio of HCl increases generally with height. The zonally averaged mixing ratio, in this particular model simulation, is slightly larger than 3 ppbv near the stratopause and less than 1 ppbv at the tropopause. It is smaller in the winter hemisphere, where a larger fraction of chlorine is tied up in $ClONO_2$. Finally, the mixing ratio of HOCl is characterized by a maximum located near 35–40 km in the tropics and subtropics, where it reaches 0.3 ppbv. The contribution of this molecule to the overall chlorine budget is therefore limited.

To provide an example of the three-dimensional evo-

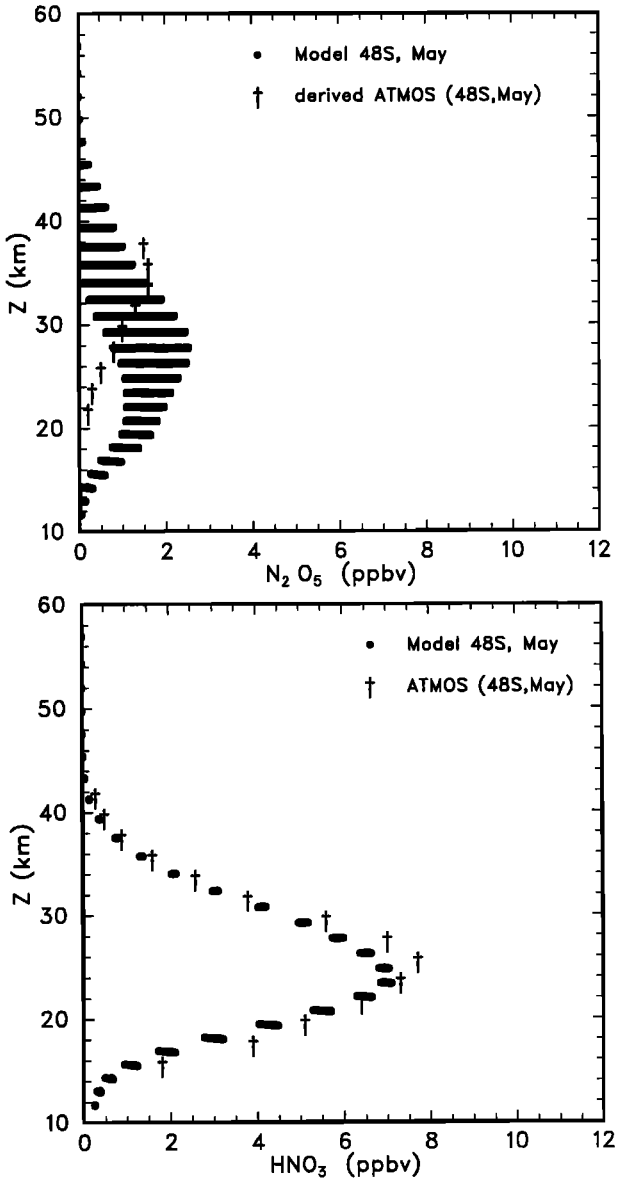

Figure 15. (top) Profiles of N_2O_5 and (bottom) HNO_3 at 48°S in May for the model and as deduced from Atmospheric Trace Molecule Spectroscopy (ATMOS).

lution of the calculated distributions of chemically active constituents, we now examine various fields on the 850 K (approximately 10 mb or 30 km) and 465K (18-20 km in midlatitudes) isentropic surfaces, respectively, over an approximate 6-week period, from March 3 to April 16. This period spans the final warming of the stratosphere as seen in the potential vorticity (PV) evolution in Plate 1. At the beginning of the period the polar vortex appears to be stable and the PV fields are nearly axisymmetric around the north pole. On March 3 a small wavenumber-1 disturbance is visible in the middle stratosphere at 850K. The wave amplifies as time evolves and becomes more noticeable on the 465K level on March 17. The structure of the PV field is completely perturbed on March 31 in the middle stratosphere (850K) with the formation of small-scale structures and intense mixing. The vortex has broken down completely. In the lower stratosphere (465K) a wave-2 component is visible, but the vortex remains well defined. By April 16, the vortex has been broken down into two distinct parts, and small-scale features are produced during this perturbed situation. At the higher level (850 K) the PV field is relatively uniform north of 40°N.

The distribution of several chemical constituents at the beginning (stable vortex) and the end (disrupted vortex) of that period will now be compared (Plate 2). The focus will first be on the middle stratosphere (on the 850K level). In the case of a long-lived species such as N_2O (photochemical lifetime of the order of 10 years at this level) the signature of the dynamical fields (e.g., PV) is clearly visible. Strong latitudinal gradients in the N_2O mixing ratio are visible at the edge of the polar vortex and into the tropics. Tongues of N_2O-rich air originating in the tropics are produced occasionally and reach subpolar regions. Such a tongue is visible on March 3 (Plate 2). At this time, the vortex appears to act as a barrier, and the mixing ratio of N_2O at the north pole (2.6 ppbv) is a factor of 40 smaller than in the subtropics (110 ppbv) and a factor of 10 smaller than outside the vortex. On April 16, as the vortex has disappeared and strong mixing has taken place, the abundance of N_2O poleward of the subtropical barrier is relatively uniform. It is now equal to approximately 40 ppbv north of 30°N and, specifically at the north pole, it is only a factor 2.5-3 lower than in subtropical regions.

The distributions of NO and NO_2 are strongly affected by photochemical processes. NO is present only during daytime and is entirely converted into NO_2 at sunset. Note that the model reproduces the rapid transition between day and night conditions without overshoots or undershoots. In the case of NO_2 the mixing ratio on the 850K level is approximately a factor of 2 higher at night than during the day. In spite of the large role played by photochemical processes, the signature of the dynamical situation is visible in the NO and NO_2 fields. The presence of the polar vortex is clearly seen on March 3, while the mixing ratios calculated for April 16 are much more uniform at high latitudes after the disappearance of the strong planetary wave disturbance. At both times, however, the effect of the NO_2 to N_2O_5 conversion is visible at middle and low latitudes. The mixing of NO_2 decreases from about 11 ppbv at sunset to 6.5 ppbv at sunrise. A compensating increase in the mixing ratio of N_2O_5 (Plate 3) occurs during the course of the night. The behavior of this latter compound is strongly affected by photochemistry at low and midlatitudes, but it is governed by dynamics in the polar region (during winter). A large gradient at the edge of the polar vortex reproduces the observed "Noxon cliff" [*Noxon*, 1979] and is only visible when the polar vortex is present. Large differences in the HNO_3 and ozone distributions are evident in comparing the fields on March 3 and April 16, respectively. A correlation between the

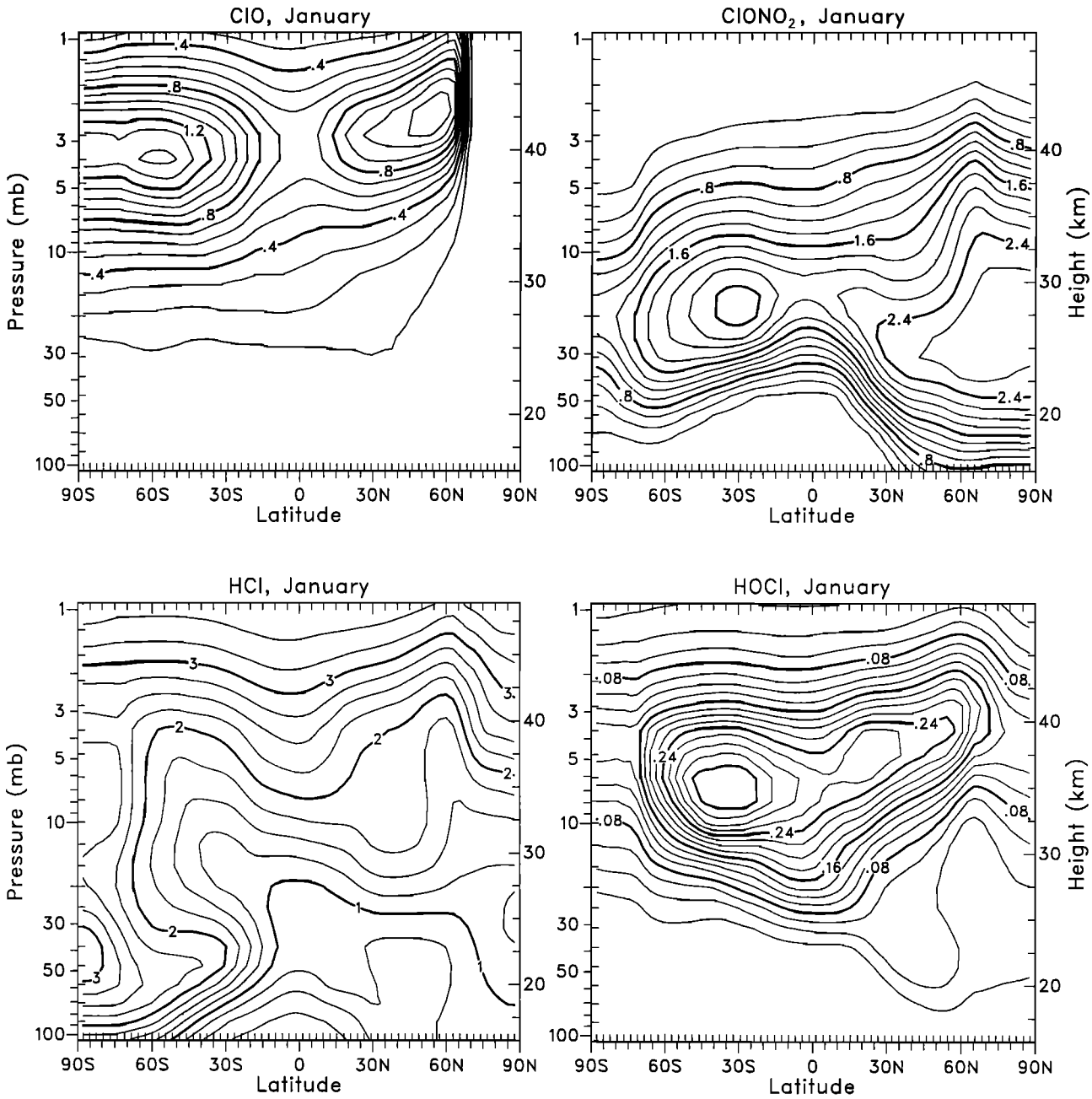

Figure 16. Model zonally averaged monthly mean values (ppbv) of some members of the Cl_x family: (top left) ClO, (top right) $ClONO_2$, (bottom left) HCl, and (bottom right) HOCl.

abundances of these two species is visible, particularly during the early stage of the time period under consideration. This result is expected to change if the heterogeneous conversion of N_2O_5 into HNO_3 on sulfate aerosol particles is taken into account.

The distributions of some of the inorganic chlorine species on the 850 K isentropic surfaces are shown in Plate 4. The strong chemical relation between ClO and $ClONO_2$ is clearly visible. After sunset, ClO is converted into $ClONO_2$ by reaction with NO_2, while after sunrise, $ClONO_2$ is rapidly photolyzed. HCl is a quasi-inert tracer and its distribution is affected mostly by dynamics. This is evident from the anticorrelation between HCl and O_3 at this level. The substantial increase seen between March 3 and April 16 is due to the descent of high HCl air during and after the warming events taking place throughout this period.

We now move to an examination of the the distribution of these same compounds in the lower stratosphere on the 465K surface in Plates 5, 6, and 7. Again, the signature of the polar vortex is visible on March 3 but has disappeared on April 16. This is reflected, for example, in the distribution of N_2O. Other features can be distinguished: while at the 850K level, the conversion between NO and NO_2 at sunset and sunrise is instantaneous; lower down at the 465K surface the transition

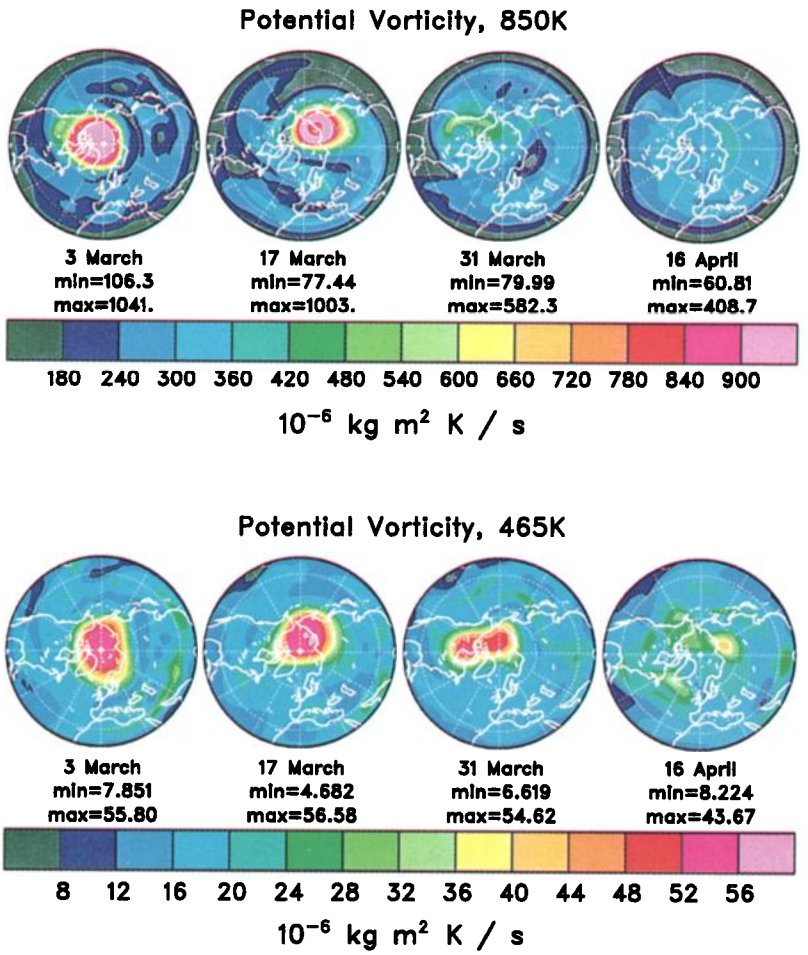

Plate 1. Potential vorticity on the (top) 850 K and (bottom) 465 K potential temperature surfaces.

is slower. There is no evidence for significant diurnal variation in N_2O_5, but the terminator is well defined on March 3, where larger values exist within the polar night. The high concentrations of N_2O_5 found in the Arctic polar night in early March have disappeared a month later, when the Sun has returned over the north pole and provided the radiation required to photolyze this nitrogen reservoir. At this level, the photolysis of chemical reservoirs (e.g., $ClONO_2$ and N_2O_5) are weaker than in the middle stratosphere, so that day-night transitions of the species are also slower than at 850K. In March the concentrations of long-lived compounds, such as HNO_3, HCl, and O_3, are highest near the north pole. In April, however, the distribution of these species has become relatively uniform as a result of the strong mixing that has occurred during the final warming event. Note again that the calculated concentration of several species near the pole would be substantially different if heterogeneous chemical processes had been taken into account. Finally, the importance of dynamical features becomes visible in the distribution of chemical tracers on the 465K level. These waves originate in the troposphere and propagate to the lower stratosphere, where they break.

5. Summary

In this paper we have presented a description of a 3-dimensional model of the middle atmosphere, which includes both a modern general circulation model and a relatively detailed model of the photochemistry important for the stratosphere. This model represents one additional step in the development of a comprehensive model capable of representing interactions between the chemistry and the dynamics of the atmosphere on multiyear timescales. Results were presented from a 2-year simulation, which included only gas phase photochemical reactions, and in which the ozone distribution forecast from the chemistry module did not affect the radiative forcing of the dynamical fields. The calculated distributions of trace species and their seasonal evolution were often quite realistic, particularly in the northern hemisphere extratropics.

Distributions of long-lived species such as N_2O and CH_4 correspond well to satellite observations. The very sharp gradient between tropics and extratropics is consistent with global observations. Polar minima are indicative of strong subsidence and correspond reasonably well to observations in the northern hemisphere. There

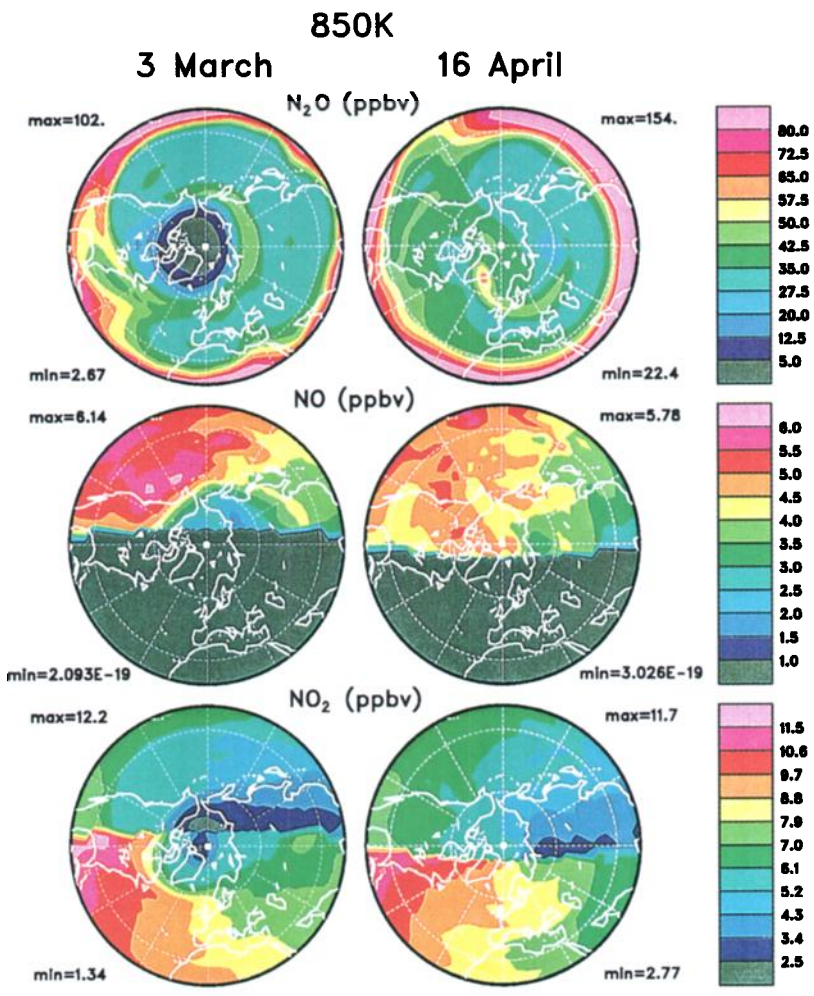

Plate 2. (top) N_2O, (middle) NO, and (bottom) NO_2 on the 850 K potential temperature surface.

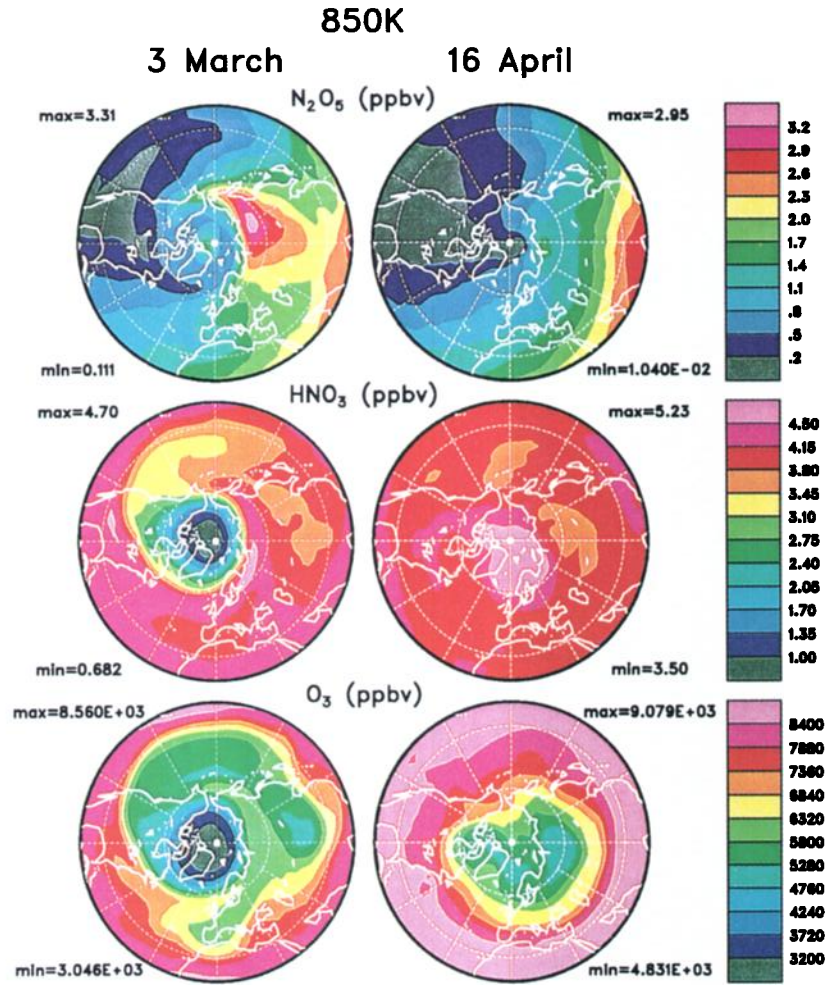

Plate 3. (top) N_2O_5, (middle) HNO_3, and (bottom) O_3 on the 850 K potential temperature surface.

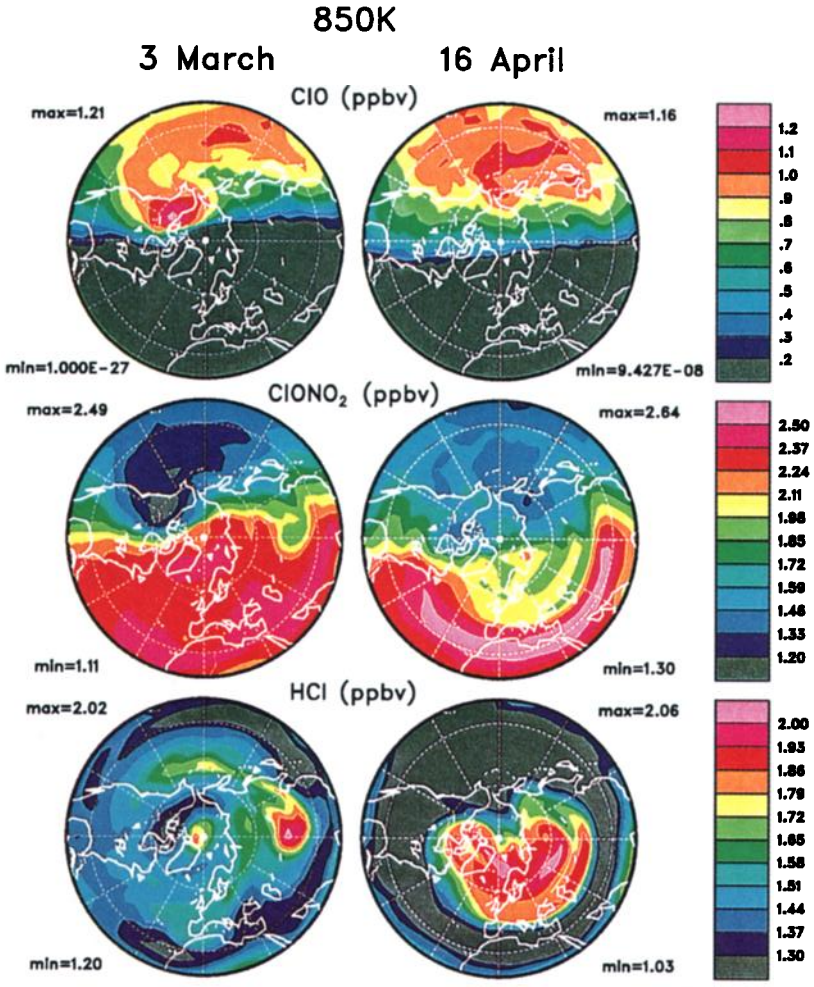

Plate 4. (top) ClO, (middle) $ClONO_2$, and (bottom) HCl on the 850 K potential temperature surface.

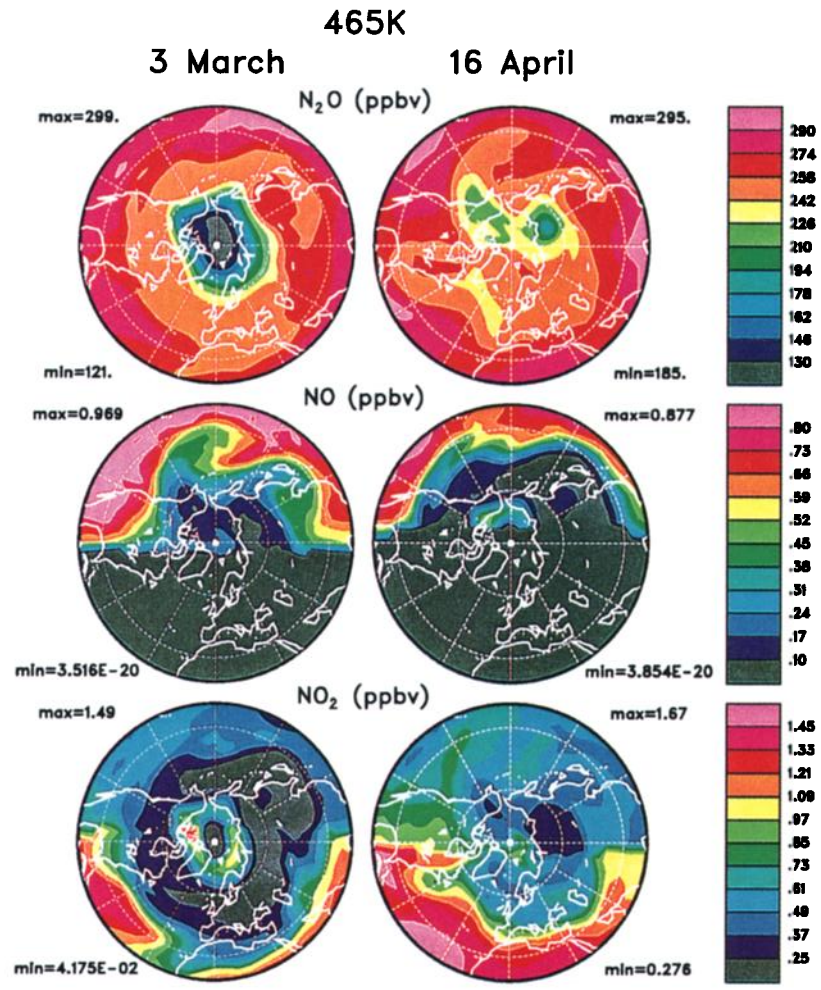

Plate 5. (top) N_2O, (middle) NO, and (bottom) NO_2 on the 465 K potential temperature surface.

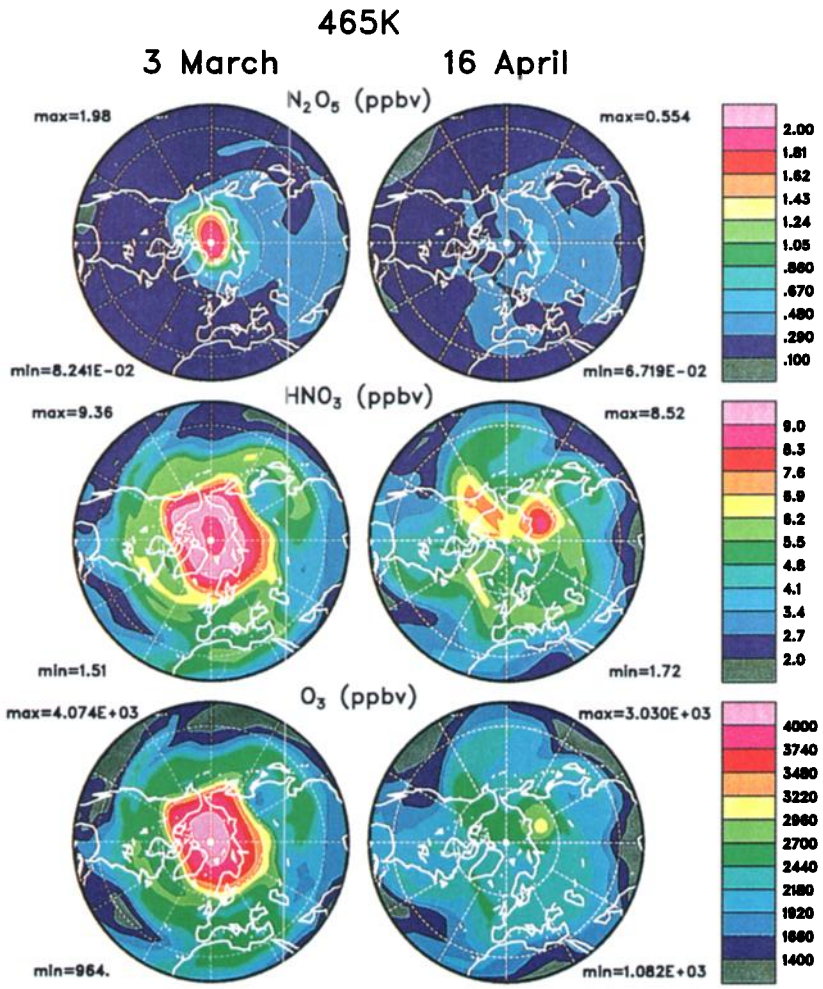

Plate 6. (top) N_2O_5, (middle) HNO_3, and (bottom) O_3 on the 465 K potential temperature surface.

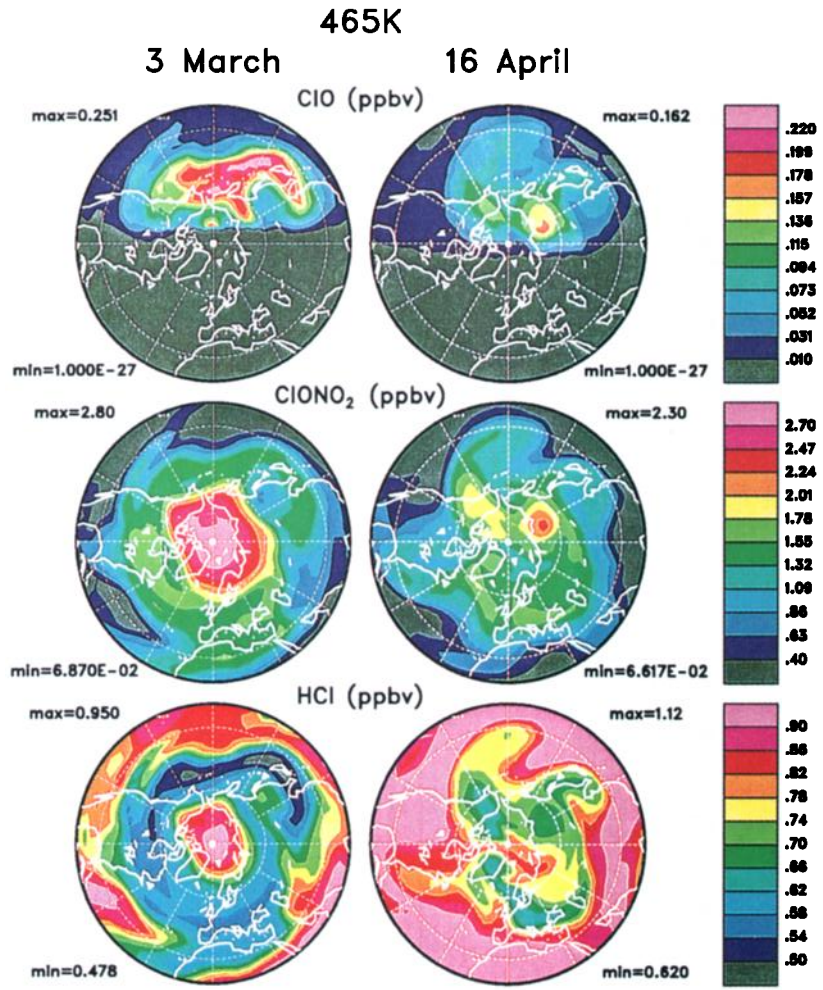

Plate 7. (top) ClO, (middle) $ClONO_2$, and (bottom) HCl on the 465 K potential temperature surface.

are also indications of some problems with the simulation: some features, such as the double-peak structure, occurring during equinoxes and commonly associated with the SAO are not reproduced; the maxima in N_2O and CH_4 are not displaced sufficiently from the equator in the summer hemisphere; density at 50 km are generally too low; and concentrations at the pole in the lowest part of the stratosphere are not sufficiently low. All of these suggest discrepancies with reality in the dynamical simulation. In particular, they suggest that the upward branch of the mean circulation is not sufficiently strong and not displaced sufficiently from the equator. On the other hand, the results indicate that in polar region the downward branch of the mean circulation occurs over too broad a region and does not descend deeply enough.

In the case of water vapor, maximum mixing ratios found in the upper stratosphere are indicative of the importance of methane oxidation processes. The dehydration in the lower stratosphere at the south pole is too strong, due to the very cold temperatures predicted by the GCM in this region. The model reproduces the large and small-scale structures in the fields of ozone and other species associated with a strong dynamical driving. The latitudinal variation and seasonal evolution of the ozone column abundance produced by the model is quite realistic, although the peak values in the spring northern hemisphere polar region are slightly underestimated. Column values in the tropics are in quantitative agreement with observations and have the correct seasonal variation. The calculated vertical distribution of the ozone mixing ratio exhibits significant differences with measured values; the model underestimates significantly the ozone density in the upper stratosphere (40 km), in part because the chlorine load adopted in the simulation is somewhat higher than the current values. The level of ClO is a factor of 2 higher than suggested by recent observations although it is only slightly higher than in 2-D model studies. The largest differences in the ozone distribution are seen in the extratropics, where the maximum values occur at too low an altitude. This feature is also seen in other long-lived species with maxima in the middle stratosphere (for example, NO_y). Finally, the model produces the key features expected in the distribution of fast reacting nitrogen and chlorine compounds when heterogeneous computers are ignored. Rapid changes, associated with fast conversion of radicals occurring at sunrise and sunset, as well as slower variations associated with the formation and destruction of atmospheric reservoirs during night and daytime are realistically simulated.

Problems in the simulation associated with the southern hemisphere circulation are pervasive. Many of these problems can be attributed to the lack of an appropriate representation of gravity waves in the model. These waves occur on smaller time and space scales than can be explicitly resolved in our model and so must be parameterized. The runs shown here currently include only a parameterization for stationary gravity waves generated through flow over orography. Parameterizations of gravity waves with nonzero phase speeds and those generated by shear and convection are not included. The model is far too cold at the winter pole during southern hemisphere winter. The polar vortex is much too persistent and far too strong, leading to a simulation looking like a perpetual ozone hole. Connected with these features are serious errors in the transport circulation. Many of these problems can be reduced by a reformulation of the gravity wave drag parameterization. This has been done, and runs are now being made with these improvements to the dynamical formulation. Results will be presented elsewhere.

In future versions of the model we intend to address other remaining model deficiencies. Some of those evident to us are as follows:

1. Heterogeneous chemistry on aerosols and polar stratospheric clouds is clearly important in the lower stratosphere. Elsewhere, we have developed representations for this chemistry [*Brasseur and Granier*, 1992; *Tie et al.*, 1994; *Lefèvre et al.*, 1994] and anticipate developing the model code along these lines in the future. Clearly, the transport and microphysical evolution of aerosols ought to be included as well. A comprehensive treatment of these processes in a 3-D model is beyond our immediate computational resources. We are exploring simplified representations for this model.

2. The prescribed values of CFCs and other halocarbons in this model resulted in higher than current-day values of Cl_x in the middle stratosphere, with some impact on the O_3 distribution. We will soon begin transporting these species in order to better predict inorganic chlorine and bromine loads in the stratosphere.

3. We have begun to run the model in a "fully coupled" mode, in which the predicted O_3 distribution is coupled with the radiative calculation. These solutions will be described elsewhere.

4. The equilibration time for H_2O in the lower stratosphere is many years. Because the model includes the stratospheric methane oxidation source and MACCM2 does not, the water vapor distribution is not yet in equilibrium. Furthermore, equilibrium values will change substantially when the gravity wave drag formulation is modified as mentioned above. The model needs to be run to equilibrium under these changed circumstances.

5. The distribution of trace species in the lower stratosphere is strongly influenced by processes occurring in the upper troposphere. Many of these processes have been treated extremely simply (e.g., washout), or neglected entirely (e.g., NO_x production by lightning). We hope to improve on this aspect of the simulation in future versions as well.

Appendix: The Modified SLT Scheme

Semi-Lagrangian transport (SLT) methods are not inherently conservative [*Rasch and Williamson*, 1990]. We enforce conservation explicitly in our model via a variational adjustment of the species mixing ratio at every time step, which we term a "fixer." The fixer weights the amplitude of the adjustment in proportion

to the advection tendencies and the field itself. The original form of the fixer is discussed by *Rasch and Williamson* [1990]. That version of the fixer was originally developed for water vapor. For species like ozone with high values in the middle atmosphere the fixer will concentrate the changes where both the tracer mixing ratio and its gradient are large (which makes sense), even if the errors in mass are generated elsewhere. This can happen because the mixing ratio must be multiplied by the density in order to calculate the mass, so that small mixing ratios (and their errors) get multiplied by large densities. The bottom line is that with the old fixer, small errors generated near the surface are corrected with larger changes high up, where the tracer is large. This problem is easily remedied by making the changes proportional to (approximately) the mass of tracer per unit volume (i.e., the density). This is achieved in the following way: let q_f be the value of the mixing ratio after fixing, q_a the mixing ratio after advection, and q_b the mixing ratio before advection; then let

$$q_f = q_a + \alpha F(\eta)|q_a - q_b|^\beta q_a.$$

α is a constant, chosen to make the mass after advection and fixing equal to the mass before, i.e.,

$$\int q_f \rho_f dV = \int q_b \rho_b dV,$$

and η is the hybrid vertical coordinate [*Hack et al.*, 1993]. In the original fixer the function F was chosen to be unity. To scale the correction approximately with density, we now let $F = \eta$ the hybrid coordinate value which is approximately proportional to pressure (and thus density). Previously, we had let $\beta = 3/2$. One can prove that in the limit of small advective tendencies (e.g., with a constant scalar field), this choice is ill-posed. The solution behaves better with the choice $\beta = 1$.

Previously, the transport scheme moved mixing ratios that had been normalized by a moist mass of air (i.e., the mass of dry air and water vapor). This means that as the water vapor of a parcel changes, its mixing ratio should change, and we had neglected this eventuality. It is easier to use a mixing ratio, which is independent of water vapor amount, and so we now transport a dry mixing ratio.

Acknowledgments. We benefited greatly from many discussions with X. X. Tie and many other colleagues and visitors to NCAR. Thanks go to Brian Eaton for programming help and to Paula Drager and Janet Rodina for editorial assistance. We thank John Gille and the Atmospheric Chemistry Division UARS group for access to the HALOE data and Jim Russell and the HALOE team for their comments and help. R. Garcia, A. Smith, and X.X. Tie helped by reviewing the manuscript. The anonymous reviewers helped significantly in improving the final version. Support for some of this work was provided by NASA grants AL72802C and W18181.

References

Austin, J., N. Butchart, and K. P. Shine, Possibility of an arctic ozone hole in a doubled-CO_2 climate, *Nature* , *360*, 221–225, 1992.

Boville, B. A., The influence of the polar night jet on the tropospheric circulation in a GCM, *J. Atmos. Sci.*, *41*, 1132–1142, 1984.

Boville, B. A., Middle atmosphere version of CCM2 (MACCM2): Annual cycle and interannual variability, *J. Geophys. Res.*, this issue.

Boville, B. A., and W. J. Randel, Observations and simulation of the variability of the stratosphere and troposphere in January, *J. Atmos. Sci.*, *43*, 3015–3034, 1986.

Boville, B. A., and W. J. Randel, Equatorial waves in a stratospheric GCM: Effects of vertical resolution, *J. Atmos. Sci.*, *49*, 785–801, 1992.

Boville, B. A., J. R. Holton, and P. W. Mote, Simulation of the Pinatubo aerosol cloud in general circulation model, *Geophys. Res. Lett.*, *18*, 2281–2284, 1991.

Brasseur, G., and C. Granier, Mount Pinatubo aerosols, chlorofluorocarbons, and ozone depletion, *Science*, *257*, 1239–1242, 1992.

Brasseur, G., M. H. Hitchman, S. Walters, M. Dymek, E. Falise, and M. Pirre, An interactive chemical dynamical radiative two-dimensional model of the middle atmosphere, *J. Geophys. Res.*, *95*, 5639–5655, 1990.

Briegleb, B. P., Delta-Eddington approximation for solar radiation in the NCAR Community Climate Model, *J. Geophys. Res.*, *97*, 7603–7612, 1992.

Cariolle, D., and M. Déqué, Southern hemisphere medium-scale waves and total ozone disturbances in a spectral general circulation model, *J. Geophys. Res.*, *91*, 10,825–10,846, 1986.

Cariolle, D., A. Lassere-Bigory, J.-F. Royer, and J.-F. Geleyn, A general circulation model simulation of the springtime Antarctic ozone decrease and its impact on midlatitudes, *J. Geophys. Res.*, *95*, 1883–1898, 1990.

Chanin, M. -L., Long term trend in the middle atmosphere temperature, in *The Role of the Stratosphere in Global Change*, edited by M. -L. Chanin, pp. 227–243, Springer-Verlag, New York, 1993.

DeMore, W. B., S. P. Sander, D. M. Golden, M. J. Molina, R. F. Hampson, M. J. Kurylo, C. J. Howard, and A. R. Ravishankara, Chemical kinetics and photochemical data for use in stratospheric modeling: Evaluation 9, *JPL Publ. 90-1*, 165 pp., Jet Propul. Lab., Pasadena, Calif., 1990.

Dickinson, R. E., A. Henderson-Sellers, P. J. Kennedy, and M. F. Wilson, Biosphere-atmosphere transfer scheme (BATS) for the NCAR Community Climate Model, *NCAR Tech. Note, NCAR/TN-275+STR*, 69 pp., Natl. Cent. for Atmos. Res., Boulder, Colo., 1987.

Eluszkiewicz, J., and M. Allen, A global analysis of the ozone deficit in the upper stratosphere and the lower mesosphere, *J. Geophys. Res.*, *98*, 1069–1082, 1993.

Garcia, R. R., Parameterization of planetary wave breaking in the middle atmosphere, *J. Atmos. Sci.*, *48*, 1405–1419, 1991.

Garcia, R. R., and B. A. Boville, "Downward control" of the mean meridional circulation and temperature distribution of the polar winter stratosphere, *J. Atmos. Sci.*, *51*, 2238–2245, 1994.

Garcia, R. R., and S. Solomon, A numerical model of the zonally averaged dynamical and chemical structure of

the middle atmosphere, *J. Geophys. Res.*, *88*, 1379–1400, 1983.

Garcia, R. R., and S. Solomon, A new numerical model of the middle atmosphere, 2, Ozone and related species, *J. Geophys. Res.*, *99*, 12,937–12,951, 1994.

Garcia, R. R., F. Stordal, S. Solomon, and J. T. Kiehl, A new numerical model of the middle atmosphere, 1, Dynamics and transport of tropospheric source gases, *J. Geophys. Res.*, *97*, 12,967–12,991, 1992.

Geller, M. A., and J. C. Alpert, Planetary wave coupling between the troposphere and the middle atmosphere as a possible sun-weather mechanism, *J. Atmos. Sci.*, *37*, 1197–1215, 1980.

Gille, J. C., and L. V. Lyjak, Radiative heating and cooling rates in the middle atmosphere, *J. Atmos. Sci.*, *43*, 2215–2229, 1986.

Goldan, P. D., W. E. Kuster, D. L. Albritton, and A. L. Schmeltekopf, Stratospheric $CFCL_3$, $CFCl_2$, and N_2O height profile measurements at several latitudes, *J. Geophys. Res.*, *85*, 413–423, 1980.

Goldan, P. D., W. E. Kuster, A. L. Schmeltekopf, F. C. Fehsenfeld, and D. L. Albritton, Correction of atmospheric N_2O data, *J. Geophys. Res.*, *86*, 5385–5386, 1981.

Grose, W. L., J. E. Nealy, R. E. Turner, and W. T. Blackshear, Modeling the transport of chemically active constituents in the stratosphere, in *Transport Processes in the Middle Atmosphere*, edited by G. Visconti, and R. Garcia, pp. 229–250, D. Reidel, Norwell, Mass., 1987.

Hack, J. J., Parameterization of moist convection in the NCAR Community Climate Model, CCM2, *J. Geophys. Res.*, *99*, 5551–5568, 1994.

Hack, J. J., B. A. Boville, B. P. Briegleb, J. T. Kiehl, P. J. Rasch, and D. L. Williamson, Description of the NCAR Community Climate Model (CCM2), *NCAR Tech. Note, NCAR/TN-382+STR*, 108 pp., Natl. Cent. for Atmos. Res., Boulder, Colo., 1993.

Hansen, J. G., G. Russell, D. Rind, P. Stone, A. Lacis, S. Lebedeff, R. Ruedy, and L. Travis, Efficient three-dimensional global models for climate studies: Models I and II, *Mon. Weather Rev.*, *111*, 609–662, 1983.

Hartley, D. E., D. L. Williamson, P. J. Rasch, and R. Prinn, Examination of tracer transport in the NCAR CCM2 by comparison of $CFCl_3$ simulations with ALE/GAGE observations, *J. Geophys. Res.*, *99*, 12,855–12,896, 1994.

Harwood, R. S., and J. A. Pyle, A two-dimensional mean circulation model for the atmosphere below 80 km, *Q. J. R. Meteorol. Soc.*, *101*, 723–747, 1975.

Hesstvedt, E., Ö. Hov, and I. Isaksen, Quasi-steady state approximations in air pollution modeling: Comparison of two numerical schemes for oxidant prediction, *Int. J. Chem. Kinet.*, *10*, 971–994, 1978.

Holtslag, A. A. M., and B. A. Boville, Local versus nonlocal boundary-layer diffusion in a global climate model, *J. Clim.*, *6*, 1825–1842, 1993.

Jackman, C. H., A. R. Douglas, K. F. Brueske, and S. A. Klein, The influence of dynamics on two-dimensional model results: Simulations of ^{14}C and stratospheric aircraft NO_x injections , *J. Geophys. Res.*, *96*, 22,559–22,572, 1991.

Jones, R. L., and J. A. Pyle, Observations of CH_4 and N_2O by the Nimbus 7 SAMS: A comparison with insitu data and two-dimensional numerical model calculations, *J. Geophys. Res.*, *89*, 5263–5279, 1984.

Kiehl, J. T., B. A. Boville, and B. P. Briegleb, Response of a general circulation model to a prescribed Antarctic ozone hole, *Nature*, *332*, 501–504, 1988.

Ko, M. W., N. D. Sze, M. Livshits, M. B. McElroy, and J. A. Pyle, The seasonal and latitudinal behavior of trace gases and O_3 as simulated by a two-dinesional model of the atmosphere, *J. Atmos. Sci.*, *41*, 2381–2408, 1984.

Kockarts, G., Absorption and photodissociation in the Schumann-Runge bands of molecular oxygen in the terrestial atmosphere, *Planet. Space Sci.*, *24*, 589, 1976.

Kodera, K., Influence of the stratospheric circulation change on the troposphere in the northern hemisphere winter, in *The Role of the Stratosphere in Global Change*, edited by M. -L. Chanin, pp. 227–243, Springer-Verlag, New York, 1993.

Kodera, K., M. Chiba, K. Yamazaki, and K. Shiba, A possible influence of the polar night stratospheric jet on the subtropical tropospheric jet, *J. Meteorol. Soc. Jpn.*, *69*, 715–721, 1991.

Le Texier, H., S. Solomon, and R. Garcia, The role of molecular hydrogen and methane oxidation in the water vapour budget of the stratosphere, *Q. J. R. Meteorol. Soc.*, *114*, 281–295, 1988.

Lefèvre, F., G. P. Brasseur, I. Folkins,, A. K. Smith, and P. Simon, Chemistry of the 1991-1992 stratospheric winter: Three-dimensional model simulations, *J. Geophys. Res.*, *99*, 8183–8195, 1994.

Mahlman, J. D., and W. J. Moxim, Tracer simulation using a global general circulation model: Results from a mid-latitude instantaneous source experiment, *J. Atmos. Sci.*, *35*, 1340–1374, 1978.

Mahlman, J. D., and L. J. Umscheid, Dynamics of the middle atmosphere: Successes and problems of the GFDL "SKYHI" general circulation model, in *Dynamics of the Middle Atmosphere*, edited by J. R. Holton, and T. Matsuno, pp. 501–526, Terra Scientific, Tokyo, 1984.

Manabe, S., and K. Bryan, Climate calculations with a combined ocean-atmosphere model, *J. Atmos. Sci.*, *26*, 786–789, 1969.

Mote, P. W., An assessment of stratospheric water vaport using a general circulation model, Ph.D. thesis, 161 pp., Univ. of Washington, Seattle, Wa., 1994.

Mote, P. W., J. R. Holton, J. Russell, and B. A. Boville, A comparison of observed (HALOE) and modeled (CCM2) methane and stratospheric water vapor, *Geophys. Res. Lett.*, *20*, 1419–1422, 1993.

Nicolet, M., Photodissociation of nitric oxide in the mesosphere and stratosphere: Simplified numerical relations for atmosphere model calculation, *Geophys. Res. Lett.*, *6*, 866, 1979.

Nicoli, M. P., and G. Visconti, Impact of coupled perturbations of atmospheric trace gases on earth's climate and ozone, *Pure Appl. Geophys.*, *120*, 626–641, 1982.

Noxon, J. F., Stratospheric NO_2, 2, Global behavior, *J. Geophys. Res.*, *84*, 5067–5076, 1979.

Pitari, G. S., S. Palermi, G. Visconti, and R. Prinn, Ozone Response to a CO_2 doubling: Results from a stratospheric circulation model with heterogeneous chemistry, *J. Geophys. Res.*, *97*, 5953–5962, 1992.

Podolske, J. R., M. Loewenstein, S. E. Strahan, and K. R. Chan, Stratospheric nitrous oxide distribution in the southern hemisphere, *J. Geophys. Res.*, *94*, 16,767–16,772, 1989.

Ramaswamy, V. M., D. Schwarzkopf, and K. P. Shine, Radiative forcing of climate from halocarbon-induced global

stratospheric ozone loss, *Nature* , *355* , 810–812, 1992.

Randel, W. J., B. A. Boville, J. C. Gille, P. L. Bailey, S. T. Massie, J. B. Kumer, J. L. Mergenthaler, and A. E. Roche, Simulation of stratospheric N_2O in the NCAR CCM2: Comparison with CLAES data and global budget analyses, *J. Atmos. Sci.*, *51*, 2834–2845, 1994.

Rasch, P. J., and D. L. Williamson, Computational aspects of moisture transport in global models of the atmosphere, *Q. J. R. Meteorol. Soc.*, *116*, 1071–1090, 1990.

Rasch, P. J., and D. L. Williamson, Sensitivity of a general circulation model climate to the moisture transport formulation, *J. Geophys. Res.*, *96*, 13,123–13,137, 1991.

Rasch, P. J., X. X. Tie, B. A. Boville, and D. L. Williamson, A three-dimensional transport model for the middle atmosphere, *J. Geophys. Res.*, *99*, 999–1018, 1993.

Rind, D., R. Suozzo, N. K. Balachandran, and M. J. Prather, Climate change and the middle atmosphere, I, The doubled CO2 climate, *J. Atmos. Sci.*, *47*, 475–494, 1990.

Rose, K., and G. Brasseur, A three-dimensional model of chemically active trace species in the middle atmosphere during disturbed winter conditions, *J. Geophys. Res.*, *94*, 16,387–16,403, 1989.

Russell, J. M., C. B. Farmer, C. P. Rinsland, R. Zander, L. Froidevaux, G. C. Toon, B. Gao, J. Shaw, and M. Gunson, Measurements of odd Nitrogen compounds in the stratosphere by the ATMOS experiment on Spacelab 3, *J. Geophys. Res.*. *93*, 1818–1736, 1988.

Russell, J. M., L. L. Gordley, J. H. Park, S. R. Drayson, A. F. Tuck, J. E. Harries, R. J. Cicerone. P. J. Crutzen, and J. E. Frederick, The Halogen Occultation Experiment, *J. Geophys. Res.*, *98*, 10,777–10,797, 1993.

Sassi, F., R. R. Garcia, and B. A. Boville, The stratopause semiannual oscillation in the NCAR Community Climate Model, *J. Atmos. Sci.*, *50*, 3608–3624, 1993.

Sellers, P. J., Y. Mintz, Y. C. Sud, and A. Salcher, A simple biospheric model (SiB) for use within general circulation models, *J. Atmos. Sci.*, *43*, 505–531, 1986.

Solomon, S., P. J. Crutzen, and R. G. Roble, Photochemical coupling between the thermosphere and the lower atmosphere, I, Odd nitrogen from 50 to 120 km, *J. Geophys. Res.*, *87*, 7206–7220, 1982.

Stachnik, R. A., J. C. Hardy, J. A. Tarsala, and J. W. Waters, Submillimeter-wave heterodyne measurements of stratospheric ClO, HCl, O_3 and HO_2: First results, *Geophys. Res. Lett.*, *19*, 1931–1934, 1992.

Stordal, F., I. S. A. Isaksen, and K. Horntveth, A diabatic circulation two-dimensional model with photochemistry: Simulations of ozone and ground released tracers, *J. Geophys. Res.*, *90*, 5757–5776, 1985.

Tie, X. X., X. Lin, and G. Brasseur, Two-dimensional coupled dynamical/chemical/microphysical simulation of global distribution of El Chichon volcanic aerosol, *J. Geophys. Res.*, *99*, 16,779–16,792, 1994.

Toon, G. C., C. B. Farmer, and R. H. Norton, Detection of stratospheric N_2O_5 by infrared remote sounding, *Nature*, *319*, 570–571, 1986.

Wang, W-C., Y-C. Zhuang, and R. D. Bojkov, Climate implications of observed changes in ozone vertical distributions at middle and high latitudes of the northern hemisphere, *Geophys. Res. Lett.*, *20*, 1567–1570, 1993.

Williamson, D. L., J. T. Kiehl, V. Ramanathan, R. E. Dickinson, and J. J. Hack, Description of NCAR Community Climate Model (CCM1), *NCAR Tech. Note, NCAR/TN-285+STR*, 112 pp., Natl. Cent. for Atmos. Res., Boulder, Colo., 1987.

World Meteorological Organization (WMO), Assessment of our understanding of the processes controlling its present distributions and change, in *Atmospheric Ozone*, vol. 1, *WMO Rep. 16*, Geneva, 1985.

Yang, H., E. Olaguer, and K. K. Tung, Simulation of the present day atmospheric ozone, odd nitrogen, chlorine and other species using a coupled 2-D model in isentropic coordinates, *J. Atmos. Sci.*, *48*, 442–471, 1991.

Yulaeva, E., J. R. Holton, and J. M. Wallace, On the cause of the annual cycle in tropical lower stratosopheric temperatures , *J. Atmos. Sci.*, *51*, 169–174, 1994.

B.A. Boville, G. P. Brasseur, P.J. Rasch, National Center for Atmospheric Research, P.O. Box 3000, Boulder, CO 80307-3000.

(Received August 3, 1994; revised December 8, 1994; accepted December 8, 1994.)